

# NUCLEAR LEVEL DENSITY, THERMALIZATION, CHAOS, AND COLLECTIVITY

Vladimir Zelevinsky<sup>1</sup> and Mihai Horoi<sup>2</sup>,

<sup>1</sup>Department of Physics and Astronomy, and National  
Superconducting Cyclotron Laboratory/Facility for Rare Isotope Beams,  
Michigan State University, East Lansing, MI 48824-1321, USA

<sup>2</sup>Department of Physics, Central Michigan University,  
Mount Pleasant, MI 48859, USA

December 3, 2018

## Abstract

The knowledge of the level density is necessary for understanding nuclear reactions involving excited nuclear states. In particular, it is an important element in description of astrophysical processes and in technological applications. This review article explains main ideas of physics forming the level density in complex nuclei that grows very fast due to combinatorial complexity of total excitation energy shared by many constituents. This can be translated into a language of statistical physics by the Darwin-Fowler method. We briefly go through the historical development from the nuclear Fermi-gas model to the self-consistent mean field including the pairing effects. At the next step we introduce the ideas of thermalization in a closed mesoscopic system and quantum chaos with very complicated eigenfunctions. This is supported by the experience of the shell model in a limited orbital space that either provides an exact solution or uses the Monte Carlo approach. The statistical method of moments allows one to avoid the exact diagonalization keeping intact the quality of the results. We discuss the popular “constant temperature model” that describes well

available data and the shell-model results; it is shown that its success cannot be explained by the phase transition from superfluid to a normal phase. The interpretation is suggested, supported by the numerical studies, in terms of dynamical chaotization including the collective enhancement of the level density. The role of incoherent collision-like interactions is stressed as a necessary element of the thermalization process.

# Contents

<b>1</b>	<b>Introduction</b>	<b>5</b>
<b>2</b>	<b>Level density: the first ideas</b>	<b>7</b>
2.1	Bethe . . . . .	7
2.2	Landau . . . . .	9
2.3	Frenkel . . . . .	11
2.4	Darwin-Fowler method . . . . .	11
2.5	Independent particle model . . . . .	14
2.6	Random spin coupling . . . . .	16
2.7	Constant temperature model . . . . .	18
2.8	First comparisons with experiment . . . . .	18
<b>3</b>	<b>Interaction effects</b>	<b>22</b>
3.1	Pairing . . . . .	22
3.2	Moment of inertia . . . . .	24
3.3	Collective enhancement . . . . .	25
3.4	Mean-field approaches . . . . .	26
<b>4</b>	<b>Monte Carlo approach</b>	<b>28</b>
4.1	Evolution in imaginary time . . . . .	28
4.2	Introducing auxiliary fields . . . . .	31
4.3	Shell-model Monte Carlo approach . . . . .	32
<b>5</b>	<b>Quantum chaos and thermalization</b>	<b>34</b>
5.1	Mesoscopic physics and quantum chaos . . . . .	34
5.2	Some measures of quantum chaos . . . . .	36
5.3	Thermalization . . . . .	38
<b>6</b>	<b>Shell model level density</b>	<b>40</b>
6.1	Briefly about the nuclear shell model . . . . .	40
6.2	Moments method . . . . .	42
6.3	Applications . . . . .	46
6.4	Role of various interaction components . . . . .	48
6.5	Comparison with Fermi-gas models . . . . .	50
6.6	Spin cutoff parameter . . . . .	52
6.7	Collective enhancement revisited . . . . .	53

<b>7</b>	<b>Constant temperature model</b>	<b>54</b>
7.1	The model . . . . .	54
7.2	Effective temperature . . . . .	57
7.3	Pairing phase transition? . . . . .	59
<b>8</b>	<b>Conclusion</b>	<b>62</b>
<b>9</b>	<b>Acknowledgements</b>	<b>67</b>

# 1 Introduction

At not very high excitation energy, an atomic nucleus is a mesoscopic system of interacting nucleons, neutrons and protons. We use here a popular word *mesoscopic* to characterize a many-body object that belongs to the world intermediate between macroscopic and microscopic “universes”. Of course, all these boundaries are quite conventional. But there are clear common features which allow to place complex nuclei, complex atoms and molecules, atomic clusters, nano-devices, and future quantum computers in the same class. In all cases we have a quantum system of a relatively small number of interacting constituents creating mean fields and many-body dynamics that lead to complexity, statistical regularities, and coexistence of single-particle and collective features. On the other hand, as the system is still not too big, it is possible to study, both in experiments and in theory, individual quantum states. This produces the wealth and depth of affable information.

The simultaneous availability of specific quantum levels and statistical features makes the theory of mesoscopic systems very rich and interesting both for applications and from the viewpoint of theoretical physics. At low excitation energy, the properties of the system are usually determined mostly by the *mean field* accumulating average features of single-particle motion, by specific correlations as *nuclear pairing*, and by low-lying *collective modes* (multipole vibrations and rotation in nuclei and molecules). Here we observe individual many-body energy levels with certain quantum numbers. With increasing excitation energy, the density of quantum states grows very fast, mainly because of the combinatorial growth of the number of possible excitations with close total energy. Although even here the individual states still can be observable, for example neutron resonances for slow neutrons interacting with heavy nuclei, this is the region where statistical concepts become extremely useful and sometimes unavoidable. An important primary example of such an approach is given by the idea of *compound nucleus* by Niels Bohr [1, 2, 3]. It is important to remember that statistical features appear in a small system with no external heat bath just due to the inter-particle interactions.

In many cases statistical arguments become the most appropriate (and often the only available), especially for experiments with limited resolution. Then one substitutes the detailed analysis with the statistical average consideration. The fundamental quantity appearing in such an analysis is the *level density*  $\rho_c(E)$  as a function of excitation energy  $E$  and exact quan-

tum numbers  $c$  for a given class of states. In nuclei  $c$  contains the total angular momentum (nuclear spin)  $J$ , its projection  $M$  onto the quantization axis, which are exactly conserved, and, approximately, isospin  $T$  (of course  $T_3 = (N - Z)/2$  is trivially conserved) and parity  $\Pi$ . Of course, the whole approach makes sense only if the close levels of the same class  $c$  have similar properties, at least with respect to a certain process under study. Then we expect that averaging over neighboring states of the same class will provide reliable generic information.

The similarity of properties of energetically close states of a given symmetry type is indeed reached through the mechanism of mixing and chaotization. Imagine a smooth changing of the interaction parameters which is easy to realize in the computational practice. If the system is stable, its energy levels smoothly evolve in this process. The stationary wave functions are mixed, especially if the levels of the same class are close in energy. The levels of the same symmetry do not cross and their minimal approach distance in energy is determined by the mixing matrix elements of the Hamiltonian. As a result of this process of *multiple avoided crossings*, we come to the strongly mixed wave functions with weakly fluctuating spacings between them (*aperiodic crystal* of energy levels). As was qualitatively formulated long ago [4], *All typical wave functions of roughly the same energy look roughly the same being spread over a large region of configuration space*. This is the situation where the statistical concept of the ensemble of close states makes clear sense and in many situations turns out to be the only possible way to describe underlying physics.

Here we do not need the exact fulfillment of the requirements of canonical random matrix ensembles [5, 6] or, more close to reality, embedded random matrix ensembles [7]. Our subject of interest, the level density, has its global behavior as a function of excitation energy and other constants of motion. This behavior is not described by the random matrices, being determined by the general evolution of the specific many-body system. If in some energy interval the states can be described by the local Gaussian orthogonal ensemble that predicts a semicircle level density (with the semicircle radius different for different classes of states) the general level density could be restored only if it would be possible to find the energy behavior and overlaps of those radii. Therefore it is more practical to consider the level density directly.

Below we present a rather short review of main ideas developed in the long search for the best description of nuclear level density, from pure phenomenology based on the semiclassical or even classical statistical considerations, up

to modern approaches using explicit nucleon interactions, known global properties of atomic nuclei and contemporary computational resources. Coming to more or less satisfactory understanding of characteristic trends and typical regularities of the density of quantum states in nuclei, one can go back and give the numerical recommendations for the values of parameters which can be practically used by experimentalists studying nuclear reactions in the laboratory, in technological applications or in astrophysical conditions. Similar approaches can be used for different mesoscopic systems.

The limited framework of this review does not allow us to review in details empirical data and applications of the level density to specific nuclear reactions. This would require another article of even greater volume. Our main subject will be the theoretical picture of various approaches to the level density, their pluses and minuses, discussion of the results and the road to current understanding of appearing regularities. Our leading direction will be the relation of the level density to underlying quantum properties of an atomic nucleus. We start with the short introduction to the work of founders (Bethe, Landau and Frenkel), then briefly explain the statistical thermodynamics in application to the level density (Darwin-Fowler method) and formulate the Fermi-gas model with later improvements. The main part of the text is devoted to ideas of quantum chaos, their typical observables in the shell-model environment (mean field, configuration interaction and statistical ways for calculating the level density – diagonalization, Monte Carlo and moments method). Finally, we discuss evolution of the level density under changes of physical parameters of interaction and the currently popular “constant temperature model”.

## 2 Level density: the first ideas

### 2.1 Bethe

Historically, the first regular approach to the nuclear level density was developed by Bethe [8] in the article called *An attempt to calculate the number of energy levels of a heavy nucleus* and summarized in the big review paper on nuclear science [9], see also [3, 10]. In fact this part of the review was a direct application of statistical mechanics to the nucleus as a bound system of many fermions, protons and neutrons. The starting point is the idea by Bohr of the compound nucleus formed after the capture of a slow neutron

which, in turn, was based on the first experiments with cold neutrons.

As the simplest image, the particles are moving inside a spherical box of a certain radius  $R = r_0 A^{1/3}$  (at that time the value of  $r_0$  was usually taken to be too large). The energy distribution of particles is given by the Fermi-statistics (borrowed from the Sommerfeld theory of electrons in metals) with certain temperature and chemical potentials. The *single-particle* level density  $\nu(\epsilon)$  in the box grows  $\propto \sqrt{\epsilon}$ . The temperature appears, by definition, as a regulator of the excitation energy needed for a given nuclear process; it is assumed to be much lower than the Fermi energy. This allows one to introduce also statistical entropy  $S$  and the level density  $\rho$  as roughly defined by  $e^S$ . Other Lagrange multipliers are required in order to fix, at least in average, specific numbers  $Z$  of protons and  $N$  of neutrons as well as the angular momentum projection  $M$  of a nucleus as a whole. As we are interested in the density  $\rho_J$  of levels with a certain value of total spin  $J$  (as characteristic for a specific experiment), a logical identity

$$\rho_J(E) = \rho(E; M = J) - \rho(E; M = J + 1) \quad (1)$$

can be applied. Theoretical studies sometimes use the minimal possible value  $M = 0$  or  $M = 1/2$  of the total spin projection; some theoretical approaches provide the *state density*  $(2J+1)\rho_J$ . As discussed by Bethe, for slow-neutron resonances on a target nucleus with total spin  $J_0$ , mainly spins  $J = J_0 \pm 1/2$  are important.

The combinatorial accumulation of states corresponding to excited particles and holes guarantees, in agreement with data, the exponential increase of the density of states. A general statistical approach based on the Darwin-Fowler method will be briefly shown in subsection 2.4, application to a Fermi-gas in subsection 2.5, and the statistical coupling of individual angular momenta in subsection 2.6.

Specific models are required in order to instill real life into a very general formalism of statistical thermodynamics. The main model used at earlier times, naturally, was that of the Fermi-gas (or two interpenetrating gases in the nuclear case) with the ground state corresponding to zero temperature. As clearly stated by Bethe, here all wealth of nuclear interactions is reduced to the formation of the potential well where the nucleons are consecutively filling single-particle orbitals. Their wave functions can be evaluated in a semiclassical approximation for a known size of the effective well. It turns out that the direct calculation along these lines with the nuclear parameters

accepted at that time leads to abnormally dense levels in the region of neutron resonances. Bethe indicated also that the actual ground state energy can be very different from that in the Fermi-gas. An interesting attempt to correct the model was made by Bardeen [11] assuming that the interaction between the nucleons effectively changes the effective mass of particles close to the Fermi surface. The second model considered by Bethe was that of a liquid drop [2] where the excited levels, at least partly, belong to the family of surface oscillations, see also subsection 2.3.

## 2.2 Landau

In his review of the level density with applications to nuclear structure and reactions, Bethe [8] considered noninteracting particles. However, some fundamental statistical properties do not depend on this assumption. According to Landau [12, 13], the nucleons form a *quantum liquid* where we expect, similarly to the electron liquid in metals and in the spirit of the latest general Fermi-liquid theory, the heat capacity growing linearly with temperature. This happens if we define the ground state temperature  $T$  equal to zero so that, at not very high excitation, the free energy of the nucleus should be

$$F(T) = -\frac{aT^2}{2}, \quad (2)$$

with a parameter  $a > 0$  roughly proportional to the particle number  $A$ . Then standard thermodynamic relations define entropy  $S(T)$  and excitation energy  $E(T)$ ,

$$S = -\frac{\partial F}{\partial T} = aT, \quad E = F + TS = \frac{aT^2}{2}, \quad (3)$$

This gives, as expected, the heat capacity linear in  $T$ . The entropy grows with energy as

$$S = \sqrt{2aE} = aT, \quad (4)$$

so that the cumulative number  $\mathcal{N}(E)$  of levels with energy smaller than  $E$  is given by

$$\mathcal{N} = e^{S(E)} = e^{\sqrt{2aE}}. \quad (5)$$

This corresponds to the *total density of states* at given energy

$$\tilde{\rho}(E) = \frac{\partial \mathcal{N}}{\partial E} = \frac{1}{T} e^{\sqrt{2aE}}. \quad (6)$$

The thermodynamic temperature is

$$T = \frac{2E}{S} = \left( \frac{\partial S}{\partial E} \right)^{-1}. \quad (7)$$

This simple approach neglects non-exponential prefactors in equations of type (5) which cannot be found without more detailed physical assumptions.

The well known criterion of degeneracy of an ideal Fermi-gas is that the de Broglie wave length of a particle is comparable with or bigger than the mean spatial distance between identical particles. This happens below the degeneracy temperature,

$$T < T_{\text{deg}} \sim \frac{\hbar^2 n^{2/3}}{m}, \quad (8)$$

where  $n = A/V$  is typical nuclear density and  $m$  nucleon mass. In nuclei not too close to drip lines,  $T_{\text{deg}} \sim 10$  MeV, and the condition (8) is fulfilled in the practically interesting region. According to Landau, the classification of states in a normal Fermi-liquid is similar to that in a Fermi-gas, at least not too far from the Fermi surface.

The next step is to subdivide the total level density into classes corresponding to certain values of the total angular momentum  $J$ . Landau assumed an analogy between the complex nucleus and a solid top. The operator  $\mathbf{J}$  has  $2J + 1$  degenerate space-fixed projections  $J_z = M$  and, approximately,  $2J + 1$  values of the  $K$  quantum number that defines the orientation of the vector  $\mathbf{J}$  in the body-fixed frame. The rotational energy is taken as

$$E_{\text{rot}}(J) = \frac{\hbar^2 J(J+1)}{2\mathcal{J}}, \quad (9)$$

with the effective moment of inertia  $\mathcal{J}$  (Landau estimated it as that of the rigid sphere with a mean nuclear radius). Then the *density of states* for a given spin  $J$  is

$$\tilde{\rho}_J(E) = \text{const} (2J+1)^2 e^{-E_{\text{rot}}(J)/T}, \quad (10)$$

where the energy-dependent normalization constant has to be found from

$$\tilde{\rho}(E) = \sum_J \tilde{\rho}_J(E). \quad (11)$$

As the states of a given  $J$ -multiplet with different values of  $M$  are strictly degenerate in the absence of external fields, the *level density* is

$$\rho_J(E) = \frac{1}{2J+1} \tilde{\rho}_J(E). \quad (12)$$

## 2.3 Frenkel

J. Frenkel [14] was seemingly the first one to indicate that the interaction between constituents in a self-bound conglomerate of particles leads to the appearance of elastic properties and *normal vibrations* in the excitation spectrum of the system. The excitation energy  $E$ , for example after the capture of an external particle by the nucleus, being spread, in the spirit of the Bohr concept of compound nucleus, over many degrees of freedom, can be interpreted as heating to a certain temperature  $T$ . In the simplest description, these degrees of freedom can be treated similarly to the Einstein model of the lattice vibrations in a solid, introducing a characteristic frequency  $\omega$ . With the number  $3A - 6$  of internal degrees of freedom, this consideration defines the relation between excitation energy and temperature,

$$E = (3A - 6) \frac{\hbar\omega}{e^{\hbar\omega/T} - 1}. \quad (13)$$

This leads to thermodynamics similar to that of simplest solids.

Certainly, this trivialized description that does not account for nucleonic degrees of freedom cannot be realistic; indeed, it predicts too long lifetimes of excited nuclei. However, this is the clear predecessor of the future idea [15] of the *collective enhancement* of the nuclear level density due to the low-lying vibrational (and rotational which are excluded from the intrinsic excitations in eq. (13) but included in consideration in the later work [16]) levels. It was also later stressed by Frenkel that the decay of a heated nucleus is resembling the evaporation from crystals; this approach is quite similar to the Weisskopf theory of the compound nucleus decay [17]. Finally, Ref. [16] contains also the idea of combining the contributions of collective vibrations and the degenerate gas of fermionic particles. In fact, the direct addition of contributions coming from nucleons and from collective modes would be wrong leading to double counting: the collective modes are coherent combinations of particle excitations; however it makes sense at relatively low excitation energy, below the main part of the typical single-particle spectrum where therefore indeed could be the collective enhancement.

## 2.4 Darwin-Fowler method

Starting from Bethe [8] physicists tried to make statistics of a degenerate Fermi gas the starting point in the search for the correct description of the

nuclear level density. The standard way to proceed is by applying the *Darwin-Fowler method* [18] usually used in the statistical thermodynamics of macroscopic systems. The thermodynamic equilibrium is defined by the maximum of entropy  $S$  at prescribed values of energy  $E$  and other fixed constants of motion  $I_i$  which, for nuclei, include total numbers  $Z$  of protons and  $N$  of neutrons, total angular momentum (nuclear spin) quantum numbers  $J, M$ , and, within certain precision, isospin  $\mathcal{T}$  and parity  $\Pi$ .

The derivation starts with the generalized statistical sum (*partition function*)

$$Z(\beta, \mu) = \sum_{E', I'} e^{-\beta E' + \beta \mu I'}, \quad (14)$$

where, for simplicity of equations, we keep only one additional constant of motion  $I$  with the Lagrange multiplier of the corresponding chemical potential  $\mu$ ; in general we would have instead the sum  $\sum_k \mu_k I_k$ . The sum (14) containing contributions of all quantum states with the values  $E'$  and  $I'$  of conserved quantities can be substituted by the integral of the formally introduced density of states  $\rho(E, I)$  with certain values of exact quantum numbers,

$$Z(\beta, \mu) = \int dE dI \rho(E, I) e^{-\beta(E - \mu I)}, \quad (15)$$

where

$$\rho(E, I) = \sum_{E', I'} \delta(E - E') \delta(I - I'). \quad (16)$$

Being a set of discrete delta-peaks, the level density becomes a smooth function of constants of motion after the minimal averaging over few neighboring levels.

The statistical mechanics, as a rule, is based on the arguments that in the statistical sum (14) the energy contributions are cut off by the exponential factor while the density of states as a function of energy grows also exponentially, see eq. (6). This competition singles out the region of energies significantly contributing to the integral and effectively makes a sharp correspondence between excitation energy and the parameter  $\beta$  establishing the temperature scale. With very fast growing level density multiplied in eq. (15) by the exponentially diminishing factor  $\exp(-\beta E)$ , the main contribution to  $Z(\beta, \mu)$  comes from the narrow region of parameters which allows us to apply the saddle point method. Introducing the free energy, or in general

an appropriate thermodynamic potential  $F(\beta, \mu)$ ,

$$F = -\frac{1}{\beta} \ln Z(\beta, \mu), \quad (17)$$

we have to evaluate the integral (15) written with the help of the level density,

$$Z(\beta, \mu) = e^{-\beta F(\beta, \mu)} = \int dE' dI' \rho(E', I') e^{\beta(-E' + \mu I')}. \quad (18)$$

The inverse Laplace transformation defines now ( $\alpha = \beta\mu$ ,  $\eta \rightarrow +0$ )

$$\rho(E, I) = \frac{1}{(2\pi i)^2} \int_{\eta-i\infty}^{\eta+i\infty} d\beta d\alpha e^{S(\beta, \alpha)}, \quad (19)$$

where thermodynamic entropy is defined as

$$S(\beta, \alpha) = \beta[E - F(\beta, \alpha)] - \alpha I. \quad (20)$$

The extremum of the entropy (20) determines the point in the space  $(\beta, \alpha)$  of the sharp maximum of the integrand (19), where

$$E = F(\beta, \alpha) + \beta \frac{\partial F}{\partial \beta} = \frac{\partial(\beta F)}{\partial \beta}, \quad I = -\beta \frac{\partial F}{\partial \alpha}. \quad (21)$$

It is easy to see that these values are in fact the mean values of the corresponding quantities in the ensemble corresponding to the thermodynamic equilibrium (the distribution function is  $\exp(-\beta E + \alpha I)$  with values  $\beta$  and  $\alpha$  taken at the extremum point). With the expansion of entropy at its extremum up to the second order, the integral (19) becomes Gaussian with the result for the level density

$$\rho(E, \{I\}) = \frac{e^{S(E, \{I\})}}{(2\pi)^{(n+1)/2} \sqrt{|\Delta|}}, \quad (22)$$

where  $n$  is the number of constants of motion  $I$ , and  $\Delta$  is the determinant of the quadratic form composed of the second derivatives of entropy at the extremum point. Using eqs. (21) we find the thermodynamic temperature

$$T_{\text{t-d}} = \left( \frac{\partial S}{\partial E} \right)^{-1} = \frac{1}{\beta}. \quad (23)$$

Strictly speaking, now one has to return to the dynamic problem for the system, namely the many-body Schrödinger equation, and calculate the partition function (14). This would open the way for finding all thermodynamic characteristics. However, the whole purpose of the statistical method is to find those characteristics avoiding the full solution of the dynamical problem. Later we will discuss various approaches to finding statistical quantities in this way. Historically the development went through the construction of gradually improved and refined models and approximations.

## 2.5 Independent particle model

This is the simplest approach modeling the system by the gas of non-interacting particles. The system is self-bound but at this stage the binding mechanism is not specified. It is sufficient to assume that the actual interaction created the mean field keeping the particles together, while the residual interaction can be accounted for at the next stage of consideration. The total wave function of any stationary many-body state is defined by the set of the occupation numbers of the single-particle orbitals  $|\nu\rangle$  with energies  $\epsilon_\nu$  in the mean field (we will distinguish occupation numbers  $n_{\nu(p)}$  for protons and  $n_{\nu(n)}$  for neutrons); in an ideal Fermi system, these occupation numbers are zero or one. Every class of nuclear states can be characterized by the constants of motion which are additive with respect to individual particles,

$$Z = \sum_{\nu(p)} n_{\nu(p)}, \quad N = \sum_{\nu(n)} n_{\nu(n)}, \quad M = \sum_{\nu} m_{\nu}, \quad (24)$$

where it is convenient to use the total spin projection  $J_z = M$  and individual projections  $j_z = m$  assuming the  $j$ - $j$  coupling scheme. Within every class, the energies of the states are additively determined by the distribution of the particles over the orbitals,

$$E = \sum_{\nu} (\epsilon_{\nu(p)} n_{\nu(p)} + \epsilon_{\nu(n)} n_{\nu(n)}). \quad (25)$$

With allowed occupation numbers 0 and 1, we come to

$$\ln Z = \sum_{\nu(p)} \ln\{1 + e^{-\beta(\epsilon_{\nu(p)} - \mu_p - \mu' m_{\nu(p)})}\} + \sum_{\nu(n)} \ln\{1 + e^{-\beta(\epsilon_{\nu(n)} - \mu_n - \mu' m_{\nu(n)})}\}, \quad (26)$$

where we introduced the chemical potentials  $\mu_p$  and  $\mu_n$  as well as the corresponding Legendre factor  $\mu'$  for the angular momentum projection. It is

assumed that we are interested in the excitation region where the energy per excited particle is still small compared to  $\epsilon_F$ . The following algebra substitutes the sums by the integrals with the corresponding average single-particle level densities  $g_{p,n}$  taken at Fermi surfaces  $\epsilon_F(p, n)$ . This set of transformations (details are easy to restore from textbooks, see for example [19]) leads to the thermodynamic potential counted from the ground state energy  $E_0$ ,

$$-F = -E_0 + \frac{\pi^2 T^2}{6} g + \mu_p Z + \mu_n N + \frac{1}{2} \mu'^2 \bar{g} T^2 \overline{m^2}. \quad (27)$$

Here the density of single-particle states can be roughly taken as  $g = g_p(\mu_p) + g_n(\mu_n)$ , while  $\bar{g}$  is averaged with respect to typical single-particle quantum numbers for protons and neutrons but still might be approximately taken equal to  $g$ . It is well known that, for one kind of particles and in the approximation of constant  $g$ , the whole problem is equivalent to the old question of the partitioning of a big integer number into a sum of smaller numbers. The solution goes back to Euler (1753) and, in the full form, to Hardy, Ramanujan and Uspensky (1918-1920).

In the same way the average value of  $\overline{m^2}$  means

$$\overline{m^2} = \frac{1}{\bar{g}} (g_n \overline{m_n^2} + g_p \overline{m_p^2}). \quad (28)$$

The total nuclear spin projection is now found as

$$M = \mu' T \bar{g} \overline{m^2}, \quad (29)$$

which essentially defines the quantity  $\mu'$  in terms of the quantum number  $M$ .

Now excitation energy of the system acquires the simple expression

$$U(T, M) = E(T, M) - E_0 = aT^2 + \frac{M^2}{2\bar{g}\overline{m^2}}, \quad (30)$$

where the standard notation giving a microscopic meaning to the Landau constant (2),

$$a = \frac{\pi^2}{6} g, \quad (31)$$

is introduced. In the same approximations one calculates the determinant  $\Delta$  in eq. (22),

$$\Delta = \frac{\pi^2}{3} T^6 g_n g_p \bar{g}^2 \overline{m^2}. \quad (32)$$

Finally, the level density of a two-component Fermi gas is given by

$$\rho(U, N, Z, M) = \frac{1}{4\pi^3} \sqrt{\frac{3g^2\bar{m}^2}{g_n g_p T^6}} e^{2\sqrt{a}\bar{U} - M^2/(2\bar{m}^2\bar{g}T)}, \quad (33)$$

A simplified expression appears if we set  $\bar{g} = g$ ,  $g_n g_p = (1/4)g^2$  and  $T \approx \sqrt{U/a}$ :

$$\rho(U, N, Z, M) = \frac{1}{12\sqrt{2}a^{1/4}U^{5/4}\sigma} e^{2\sqrt{a}\bar{U} - M^2/2\sigma^2}, \quad (34)$$

The spin projection  $M$  has a Gaussian distribution with the width  $\sigma$ ,

$$\sigma^2 = g\bar{m}^2\sqrt{\frac{U}{a}} \approx gT\bar{m}^2. \quad (35)$$

Here we can mention that the computational problem of calculating the level density of independent fermions for a given set of single-particle energies  $\epsilon_a$  can be easily formulated in terms of the Fourier components in real time [20]. Indeed, using the Fourier transformation

$$\rho(E) = \text{Tr}\{\delta(H - E)\} = \int_{-\infty}^{\infty} \frac{dt}{2\pi} e^{iEt} G(t), \quad (36)$$

where

$$G(t) = \text{Tr}\{e^{-iHt}\}, \quad (37)$$

we come to the product over all available single-particle levels labeled  $a$  with occupancies  $n_a$  equal 0 or 1:

$$G(t) = \prod_a (1 + e^{-i\epsilon_a t}). \quad (38)$$

This can be generalized to the subsets of states with given *additive* quantum characteristics, such as proton and neutron numbers, and the projection  $M$  of angular momentum, see the next subsection. Then the fast Fourier transform delivers the level density (36).

## 2.6 Random spin coupling

The Gaussian  $M$ -distribution found above can be derived [8] avoiding the whole Darwin-Fowler machinery just as a result of the random coupling of

angular momenta of individual particles,  $M = \sum_a m_a$ . When we allow for many levels of a complex system to result from numerous superpositions of individual, let say single-particle, excitations, the majority of such combinations correspond to more or less chaotic couplings of spins and orbital momenta of participants. Then the famous central limit theorem of probability theory enters the game and the distribution tends to the Gaussian.

With  $w_N(M)$  defined as a probability of the total angular momentum projection of  $N$  particles to be equal to  $M$ , the logical identity should be valid for the process of random addition of individual spins,

$$w_N(M) = \sum_{M'} w_n(M') w_{N-n}(M - M'). \quad (39)$$

Here we use the fact that individual projections are added algebraically; the division into groups of  $n$  and  $N - n$  spins is arbitrary which characterizes a discrete Markovian process. In the supposed absence of interference in angular momentum addition, the combined quantities are probabilities rather than amplitudes. Going further along this path, one substitutes the sum in eq. (39) by an integral and comes to the Gaussian solution,

$$w_N(M) = \sqrt{\frac{\alpha}{N\pi}} e^{-\alpha M^2/N}, \quad (40)$$

where  $\alpha$  is determined by the properties of the system, namely by the average value

$$\overline{M^2} = \frac{N}{2\alpha}. \quad (41)$$

The number

$$N(E) \approx gT(E) \quad (42)$$

of active constituents is determined, as in the previous section, by the single-particle density of states  $g$  at the Fermi surface. In the simplest consideration, the width  $\sigma_m$  of the Gaussian (40) is defined by single-particle spins  $j$  present in a given orbital space:

$$\alpha = \frac{1}{2\sigma_m^2} = \frac{1}{2m^2}; \quad \overline{m^2} \approx \frac{1}{3} \overline{j(j+1)}. \quad (43)$$

Here possible correlations of individual spins are neglected. The level density as a function of energy and spin projection  $M$  is similarly to Eq. (10),

$$\rho(E; M) = \rho(E)w(M, E). \quad (44)$$

## 2.7 Constant temperature model

The whole situation in the problem of nuclear level density and, more general, of statistical features in nuclear structure and reactions, was reviewed and summarized in an influential article by Ericson [21] based on the several previous publications [22, 23, 24, 25]. In our review we discuss essentially only the level density part. As the main ideas of this period were already outlined above in the same spirit as in [21], in this subsection we limit ourselves by one comment important for the future discussions.

Ericson's characteristic of the whole level density problem starts with the statement that the level density, according to the sets of data available at that time, is in fact an exponential function of energy. The examples shown in [21] are given for few specific nuclei ( $^{33}\text{S}$ ,  $^{55,57,58}\text{Fe}$ , and  $^{56}\text{Mn}$ ) and excitation energy up to several MeV. The exponential behavior starts at the excitation energy about 1 MeV, and even below that in odd-odd nuclei. At the same excitation energy, the level density  $\rho(E)$  and its integral, the cumulative state number  $\mathcal{N}(E)$ , is bigger for the odd-odd case as it is expected from the viewpoint of the pairing interaction, see below. The dependence on energy can be depicted as proportional to  $e^{E/T}$  where the parameter  $T$  looks as some kind of temperature but here it is just a constant. Correspondingly, this fit gave rise to the so-called *constant temperature model* (CTM) that became one of the main models on the market much later. With incomplete experimental material, it was hard to make a choice between the Fermi-gas description and the CTM. We should mention that the spin distribution is preserved as in the previous subsection.

The serious work comparing the Fermi-gas predictions with the CTM was performed in [26, 27]. The best description can be reached assuming the CTM at relatively low energy,  $E \leq 10$  MeV, and smoothly attaching this to the Fermi-gas description with  $\rho \propto e^{\sqrt{2aE}}$  at higher energies; the details of the matching procedure can be found in [28]. In [27], the list is given of recommended parameters for many known at that time isotopes from  $^{63}\text{Zn}$  to  $^{245}\text{Cm}$ . This formulation, being well reproduced by the shell model diagonalization, will reappear in our review later.

## 2.8 First comparisons with experiment

The approaches delineated above were immediately used by many experimentalists as an instrument for ordering their data and systematizing the

behavior of the level density along the nuclear chart. The typical sources of the data are the spectroscopy of low-lying states and the region of neutron resonances at excitation energy of 7-10 MeV. Having in mind the Fermi-gas picture at temperature  $T$  much lower than the Fermi energy, one can use the number of particle-hole excitations derived by the integration around Fermi surface,

$$\bar{n} = 2\bar{g} T \ln 2 \approx \sqrt{aE}, \quad (45)$$

and the mean energy per excitation as  $\bar{\epsilon} = E/\bar{n} \approx T$ . The quantity  $T = \sqrt{E/a}$  is traditionally called *thermodynamic temperature* being estimated from the data as 0.5-1 MeV at excitation energy of neutron resonances. The level density parameter  $a$  can be extracted from evaporation spectra of a compound nucleus using the detailed balance relations [29]. Slightly different versions of the Darwin-Fowler method and of the spin effects were provided by Bloch [30] with a more accurate account of the actual spectrum of the nucleons in a central potential and rough estimates of residual forces, but the results were not significantly different. Finally, allowing the level density parameter  $a$  to slowly vary with temperature one can get a rather good agreement with the neutron resonance data [31].

It was understood that the prediction of the dependence on the mass number due to the spatial inflation of the nucleus,  $a \propto A^{2/3}$ , is a serious simplification that neglects the shell structure of the nuclei. This structure is not only seen in the shell modulation of the parameter  $a$  but it also depends on the composition of the single-particle orbitals inside each shell [32, 33] in the interval of the order of temperature around the Fermi-surface. Combinatorial arguments speak in favor of the increase of the level density (in terms of the parameter  $a$ ) in the middle of shells or subshells (Rosenzweig effect [34, 35]). We can also mention that the modified Darwin-Fowler procedure [40] that changes the equation of state  $E = aT^2$  to  $E = aT^2 - T$  was shown to be incorrect [26, 27]. The detailed comparison with available data was made [41, 42] by the Soviet physicist Malyshev who has early passed away.

The spin dependence of the level density turned out to be in general consistent with the Fermi-gas approach and the idea of random coupling of individual spins taking into account the realistic shell structure [30]. The spin-orbit coupling, with the sign opposite to such a coupling in atomic configurations, removes the harmonic oscillator degeneracy and changes the ordering of single-particle orbitals, observed magnetic moments etc. The serious analysis of the spin dependence was performed in [43, 44] on a large experimental

material for odd-odd isotopes  $^{24}\text{Na}$  and  $^{28}\text{Al}$ . The capture reactions with thermal neutrons [45] and other reactions with the compound nucleus formation [46] confirmed the spin dependence in the form  $\exp[-(J+1/2)^2/2\sigma^2]$  that follows approximately from eqs. (1) and (42); the typical values of the parameter  $\sigma$  were found to be around 4. The useful information was obtained from reactions populating isomeric states with different spin values [47]. The direct extraction of the spin dependence from angular distributions of particles emitted by compound nuclei [48, 49] was at that time not very reliable.

In practice, neutron reactions at low energy provide information only for  $s$ - and  $p$ -resonances. In order to find the basic parameter  $a$ , one needs to know the mean value  $\overline{m^2}$ , eq. (43). The averaging can be done in different ways but a relatively good description using the shell-model level sequences close to the Fermi energy is given by assuming [50]

$$\overline{m^2} = 0.146 A^{2/3}; \quad (46)$$

(semiclassical estimates lead to a higher value of the numerical coefficient). This determines the spin dependence parameter (35)

$$\sigma^2 = 0.089 \sqrt{aE} A^{2/3}. \quad (47)$$

Because of the dominance of  $s$ -resonances, additional assumptions are needed to account for the levels of opposite parity. It was usually accepted that at such excitation energy both parities are equiprobable. This assumption did not contradict available at that time data.

Quite early it was understood [51] that the quality of information extracted from neutron resonances depends on the resolution and probability of missing weak resonances. Here the help came from the statistical treatment of resonances. This is important when we come to the notion of quantum chaos and its reflection in the level density. But already the simplest ideas of mixing the complicated wave functions of a compound nucleus lead to the assumption of a random (Gaussian) distribution of the amplitudes of individual shell-model components in such a typical state. Introducing the reduced widths  $\gamma = \Gamma/\bar{\Gamma}$ , where the energy dependence of the width growing with the distance from threshold is excluded, we can assume that these reduced widths are proportional to squares of the corresponding amplitudes in a complicated wave function and follow the chi-square distribution for one

degree of freedom. This is usually called the *Porter-Thomas distribution*,

$$f_{\text{PT}}(\gamma) = \frac{1}{\sqrt{2\pi\gamma}} e^{-\gamma/2}. \quad (48)$$

Experimental and theoretical discussions on the applicability of Eq. (48) are still going on, see [141] and references therein. The distribution of spacings  $s$  between the closest levels with the same exact quantum numbers is described by the Wigner formula,

$$P(s) = \frac{\pi s}{2} e^{-\pi s^2/4}. \quad (49)$$

A characteristic feature here is the linear repulsion of levels at small distances telling about the mixing of underlying wave functions which makes the sequence of states with the same exact quantum numbers kind of an aperiodic crystal (the level repulsion was first discussed in [52]). The effective spacing  $s$  in eq. (49) is taken in the units of the local mean level spacing that evolves with the level density. The real experimental problem is to distinguish weak  $s$ - and  $p$ -resonances. One can conclude that the parameter  $a$  is determined from the resonance information within the interval of 10-15%.

The neutron reactions proceeding through a compound stage allow to determine the kinetic energy spectrum of evaporated neutrons. Using the detailed balance principle and assuming the Maxwellian neutron spectrum one can find out the effective temperature of the residual nucleus. This parameter defined by the level density of the final nucleus is called *nuclear temperature*  $T_n$ . Its difference from the thermodynamic temperature (23) is essentially determined by the pre-exponential factors in the Darwin-Fowler formulation. For the Maxwellian spectrum, mean energy carried by an evaporated neutron equals to  $2T_n$ . As can be found from (34) (see for example [53]),

$$T = \frac{T_n}{1 + (5T_n)/(4E)}, \quad (50)$$

and the difference goes away at sufficiently high excitation energy.

The general conclusion at this stage of the development is [54] that the parameter  $a$  has to be adjusted for individual nuclei and neither its value nor its evolution along the nuclear chart are completely understood.

## 3 Interaction effects

The nucleons interact which is necessary to create a self-bound nuclear drop. There are parts of the interaction appearing on top of the mean field background that lead to inter-particle correlations. It was usually claimed that *incoherent* (collision-like) interactions between the particles in the shell-model framework do not seriously influence the resulting level density serving first of all as an agent leading to thermal equilibrium. Later we will see that the exact solution of the shell model (configuration interaction) modifies this conclusion. However it was quite early understood that *coherent* interactions are certainly important: the phenomena of collective character significantly change the Fermi-gas picture. First we indicate the main qualitative novelties.

### 3.1 Pairing

The well known effects of the deeper binding of even-even nuclei compared to odd- $A$  and odd-odd ones, along with the suppressed level density at low excitation energy in spherical even-even nuclei, immediately indicate the presence of an extra attraction between a pair of nucleons occupying time-conjugate orbitals. This was assumed already by the founding authors of the shell model [55, 56] in order to predict the ground state spins and magnetic moments of odd nuclei as defined by the  $j$ -value of the last unpaired nucleon. After appearance of the Bardeen-Cooper-Schriffer (BCS) theory of superconductivity [57], the idea was formulated by A. Bohr, Mottelson and Pines [58] of similar pairing physics at work in complex nuclei. The theory of the nuclear pairing correlations of superconducting type was developed by Belyaev [59] on the base of the Bogoliubov canonical transformation. It was demonstrated that not only single-particle characteristics of a complex nucleus are considerably modified by pairing correlations but the pairing leads also to strong changes of collective properties. In spherical nuclei, low-lying vibrational modes, usually of quadrupole character, appear, while in well deformed nuclei the rotational bands have typically the moment of inertia noticeably smaller than the moment of inertia of a rigid body of the nuclear mass and size.

The first consequence of pairing correlations of superconducting or superfluid type is the appearance of the energy gap  $\Delta$  in the spectrum of single-particle excitations of even subsystems (breaking of pairs with isospin

1). In the simplest version of the theory, the Fermi-gas spectrum  $\epsilon_\nu$  changes to

$$E_\nu = \sqrt{\epsilon_\nu^2 + \Delta^2}, \quad (51)$$

where the shell energy  $\epsilon_\nu$  is counted from the chemical potential (practically equal to the Fermi energy, separately for protons and neutrons). The quantity  $\Delta$  can serve as a measure of even-odd mass difference [60]. An important result of Ref. [61] was that the fluctuations in the measured radiation widths of neutron resonances are small compared to the large fluctuations in neutron scattering widths, and that they are related to the level spacing and the effective level excitation energy. The simplest way to account for pairing is to define the excitation energy subtracting the effective gap energy  $\Delta_p$  or  $\Delta_n$  in the case of an odd number of protons or neutrons, respectively, while for even-even nuclei this shift is  $\Delta_p + \Delta_n$ . This was a justification of the popular *back-shifted Fermi gas formula* [27, 62], explicitly modifying eq. (34) by introducing a free parameter of energy displacement,

$$\rho(U, N, Z, M) = \frac{1}{12\sqrt{2}a^{1/4}(U - \Delta)^{5/4}\sigma} e^{2\sqrt{a(U-\Delta)-M^2/2\sigma^2}}, \quad (52)$$

For the excitation energy below the shift  $\Delta$ , one can count the levels directly if the empirical information is available. In practice, the three parameters entering this description for each nucleus,  $a$ ,  $\sigma$ , and  $\Delta$ , can be allowed to slightly change with energy as discussed in more detail in [28, 63]. Such variations supposedly reflect the absent in phenomenology shell and collective effects, see the compilation in [64]. The review of this approach can be found in [65].

The empirical expressions [60] can include also differences in surface, symmetry, and Coulomb energy from the nuclear mass curve. Such recipes allow one to approximately reconcile the values of the parameter  $a$  for different groups of nuclei. The reasonable linear description that averages the shell oscillations corresponds to  $a \approx 0.125A$ . One can disentangle this dependence interpreting the factor  $A^{2/3}$  as coming from the size of the upper shell of the nucleus and  $A^{1/3}$  from the increase of the mean angular momentum  $j$  of the nucleons occupying this shell. The specific shell structures are responsible for oscillations around this line. We can also mention that later it was found [66] that the empirical value of the level density parameter  $a$  can depend on the distance of the nucleus from the line of stability, which can be approximately

expressed with the help of the factors  $\alpha$  and  $\beta$ :

$$a = \alpha A e^{-\beta(N-Z)^2}. \quad (53)$$

This can be naturally related to a greater set of allowed isospin values at  $N = Z$ . Later we will see this effect in the CTM.

The analogy to macroscopic superconductivity however cannot be literally right due to the smallness of nuclear systems (a formally calculated coherence length of Cooper pairs is greater than the nuclear size). Therefore, for example, instead of the phase transition to the normal phase [57] at the BCS critical temperature  $T_c = \Delta(T = 0)/1.75$ , the shell-model analysis shows [67] a smooth crossover with the gradually decreasing gap in all sectors with different total spins. The level density, being in even-even nuclei quite small below  $E \approx 2\Delta$  (only collective states), becomes large above this threshold accumulating single-particle excitations pushed up from the gap. Then at  $E \approx 4$  MeV, the observed level density is getting comparable to the Fermi-gas predictions.

### 3.2 Moment of inertia

In the thermodynamic derivation of the level density (34), the term depending on the angular momentum projection  $M$  can be interpreted as the effective rotational energy [48]. If, in the semiclassical spirit, it is considered as a regular part of total energy corresponding to a non-statistical rotation, it should be subtracted from the total excitation energy. In this approximation,

$$\rho(E, M) \approx \rho(E'_M, 0), \quad E'_M = E - \frac{\hbar^2 M^2}{2\mathcal{J}}, \quad (54)$$

where  $\mathcal{J} = \overline{gm^2}$  is an average moment of inertia. As rotational energy is a small part of the total excitation energy, one can use the expansion in eq. (54) and come to

$$\rho(E, M) \approx \rho(E, 0) e^{-\hbar^2 M^2 / (2\mathcal{J}T')}, \quad (55)$$

with a slightly different effective temperature

$$T' = \left[ \frac{d}{dE} (\ln \rho(E, 0)) \right]^{-1}. \quad (56)$$

This leads to the redefinition

$$\sigma^2 = \frac{\mathcal{J}T'}{\hbar^2}. \quad (57)$$

It is easy to show ([68], Section 16.20) that, in the semiclassical consideration, the moment of inertia of a normal Fermi-system is given by the classical expression for a body with the same density distribution,  $\mathcal{J} = \mathcal{J}_{\text{cl}}$ ; a general theorem can be found in [69]. The earlier found expression (35) does not numerically agree with the rigid-body moment of inertia, eq. (57). As shown in Ref. [59], pairing correlations noticeably reduce the nuclear moment of inertia of well deformed nuclei with clearly visible low-energy rotational bands. With growing excitation energy, the pairing effects are gradually melted, and characteristic values of the moment of inertia also grow approaching the rigid-body limit. In spherical or weakly deformed nuclei, the simple rotational bands are absent, the sequence of the spin values is not so well defined which brings also isomeric effects. Here we expect to have in expressions like (57) some effective mean moment of inertia. For strongly deformed and non-axially symmetric nuclei, the different moments of inertia corresponding to the rotation around different axes, give separate contributions to equations of type (55). At the relatively early stage of development, the whole picture of rotational bands and effective moments of inertia was not that clear.

### 3.3 Collective enhancement

The residual interactions, on top of the shell model and pairing, introduce coherent motion of particles. As a result, the spectrum of stationary states includes collective, vibrational and rotational, levels. If the interaction has an attractive character, resulting vibrational modes, first of all of quadrupole type, have low energy, typically well inside the pairing energy gap. In the low-lying part of the spectrum, these states can be roughly classified in terms of *phonons*, collective superpositions of several elementary particle-hole (two-quasiparticle in the presence of pairing) excitations; recall Section 2.3 where they were treated as bosons specified in a liquid drop model [2] as surface vibrations of certain multipolarity. Actual collective vibrational states have energy inside the pairing gap, enhanced electromagnetic transition rates and usually are characterized by strong anharmonicity, both due to the Pauli principle between the fermionic constituents and due to the mixing with non-collective states. The collective rotational states just slightly perturbing

intrinsic correlations have energy even lower than vibrations. With respect to the ground state, both types can be expressed as coherent linear combinations of basic particle or quasiparticle excitations. As a result, the density of low-lying states increases slightly compensating the absence of simple particle-hole states inside the gap and leading to the so-called *collective enhancement* [15] of the level density. It is especially pronounced above the gap in deformed nuclei where numerous rotational bands start being built on unpaired configurations.

Phenomenologically, the collective enhancement can be accounted for by an additional energy-dependent factor [28]. Of course, in any finite orbital space, the surplus of states at relatively low energy should be compensated by the exhaustion of states somewhere higher up but in real life this “fading out” was never reliably observed due to the available higher shells. However, as we will see later, the effect of collective enhancement can be studied with the help of the shell model. It is quite important for the description of fission where only a two-center shell model with its wealth of collective modes can hopefully give a real microscopic foundation. The incomplete information on the density of neutron resonances traditionally used for extraction of the level density is accumulated in the RIPL-2 database [70], see also [28].

### 3.4 Mean-field approaches

The microscopic approaches based on the Fermi motion in a self-consistent mean field can be developed in the spirit of energy density functionals, first of all of Skyrme-type, giving rise to *microscopic combinatorial models* described in [71, 72]. The combinatorial method by itself is a generalization of the simple formulation (36) when the mean-field energies are found as those of single-particle excitations generated by a full Hamiltonian of inter-particle interactions. The many-body states considered as actual excitations of the system are found by exact combinatorics counting all possibilities up to a certain limit. Essentially the result is the cumulative number of states with an angular momentum projection  $M$  (and given parity) up to a total energy  $E$ . Of course, our rough description does not mention many specific tools and approximations used in practical calculations.

The mean field is determined in the Hartree-Fock-Bogoliubov (HFB) approximation. In the HFB method, the single-particle density matrix of the ground state includes, on top of the usual matrix elements  $\sim a^\dagger a$ , also pairing parts  $\sim aa$  and  $\sim a^\dagger a^\dagger$  which are found self-consistently, see for example

[73, 74]. This means that the total particle number is not preserved exactly; instead it is regulated in average by the chemical potentials for protons and neutrons.

The definition of the vibrational states appearing inside the pairing gap as an important part of the collective enhancement requires to go beyond the mean field level using the time-dependent density matrix or the random phase approximation. Instead the problem can be circumvented by adding the vibrational (quadrupole and octupole) states on top of the mean-field states but only up to some excitation energy in order to avoid double counting. The equilibrium axial deformation is selected by minimizing the ground state energy, while the effective moment of inertia for collective rotation around the axis perpendicular to the symmetry axis can be calculated by the cranking model [78]. The whole procedure becomes less definitive for soft spherical or transitional nuclei. In general, the applications contain a number of approximations and simplifications. The results typically give the density of neutron resonances higher than in reality.

The further development of this approach [79] provided the level densities for more than 8500 nuclei. Still the three main components in the play are single-particle shell model level schemes, pairing and collective effects. The first two parts of the approach construct the basic level sequence. The collective enhancement is determined by the explicit consideration of vibrational states counted as independent bosons [72] with their maximum number equal to three in spherical or axially symmetric deformed geometry. As in the earlier work [80], the phonon frequencies for multipolarities  $\lambda = 2, 3, 4$  were either described phenomenologically with the general dependence  $\propto A^{-5/6}$  and some shell corrections, or taken from the data. One needs also a recipe for avoiding the double counting of states included both in the vibrational enhancement and in the single-particle part (damping of the collective enhancement factor). For deformed nuclei, the rotational bands are constructed on intrinsic states assuming the axial deformation and rigid-body moment of inertia; a phenomenological interpolation is introduced describing the possible transition to spherical shape at higher energy. Frequently, instead of the originally applied Gogny force, some versions of the Skyrme functional are used. Special efforts were applied to describe the level density at the fission saddle point which is outside of our review. The resulting comparison with experimental data can be illustrated by Figure 1 taken from Ref. [79]. Although the qualitative behavior of theoretical predictions is quite reasonable, there are significant deviations even at low energy seen even with the

logarithmic scale.

At the next step [81], the new Gogny interaction was used [82] optimized for the description of binding energies although still the collective energies are overestimated which requires introduction of special renormalizations. A new concept here is the introduction of the shape transition from deformed to spherical at higher energy through the temperature-dependent HFB approach. Along with that, the rigid body moments of inertia are substituted by the microscopic ones. Special efforts are needed in order to smooth a discontinuity appearing between the level densities calculated at different discrete temperatures. One can judge on the quality of the level density reproduction from Figure 2 (taken from Ref. [81]). For the cumulative level number the deviations are even more noticeable; in many cases the observed data behave more smoothly than it is predicted by the combinatorial method. Some deficiencies of this approach, which certainly at a time of its development filled in an important niche, will be indicated later.

## 4 Monte Carlo approach

### 4.1 Evolution in imaginary time

The Monte Carlo methods in application to nuclear structure exist in various modifications [83, 84, 85]. The detailed introduction to their use in the nuclear shell model context can be found in [86]. The general idea, common for different versions, is to substitute the diagonalization of prohibitively huge Hamiltonian matrices by statistical consideration. This is achieved by looking into quantum evolution driven by the operator  $e^{-iHt}$  (in units with  $\hbar = 1$ ) for imaginary “time”,  $t \rightarrow -i\beta$ , where  $\beta$  is a real positive parameter. The resulting operator  $e^{-\beta H}$  describes the equilibrium quantum ensemble with the effective temperature  $1/\beta$ . The limit  $\beta \rightarrow \infty$  selects from any superposition of stationary states of the Hamiltonian  $H$  the component of this superposition with the lowest energy (cooling the system). In the context of the level density this is one of the necessary steps as the knowledge of the ground state energy is required for the correct placing the level density; however, there are technical problems in the limit  $\beta \rightarrow \infty$ .

We assume that the Hamiltonian of the many-body system can be ex-

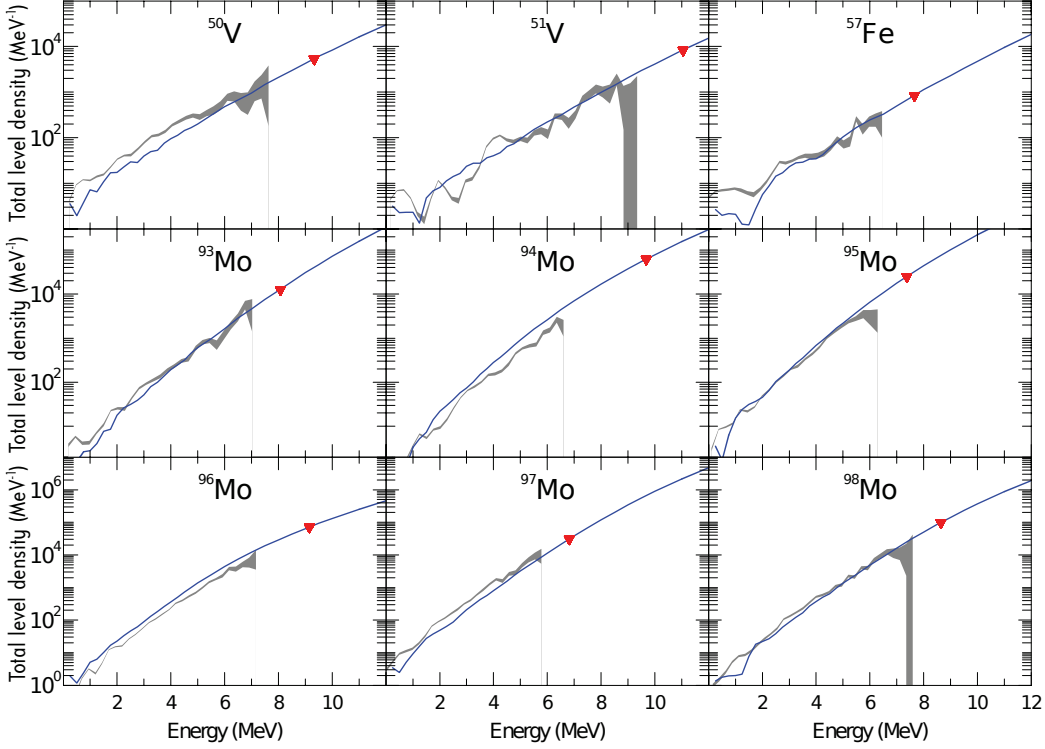


Figure 1: Comparison between the total level density determined by the Oslo group (gray areas) and the HFB combinatorial predictions (solid lines). The full triangles correspond to the model-dependent normalization point derived from the average neutron resonance parameter value at the excitation energy of neutron separation threshold. Figure reproduced from Ref. [79].

pressed in terms of linear and quadratic combinations of one-body operators

$$\hat{Q} = \sum_{12} Q_{12} a_1^\dagger a_2 \equiv \sum_{12} Q_{12} \hat{O}_{12}, \quad (58)$$

where the subscripts 1, 2, ... run over all single-particle states, while  $a^\dagger$  and  $a$  are corresponding fermionic creation and annihilation operators in a certain single-particle basis. The two-body interaction Hamiltonian is presented as a sum of terms

$$H_j = \epsilon_j \hat{O}_j + \frac{1}{2} g_j \hat{O}_j^2, \quad (59)$$

where  $g_j$  are coupling constants. The specific representation of the actual two-body Hamiltonian in the form (59) can be performed in different versions,

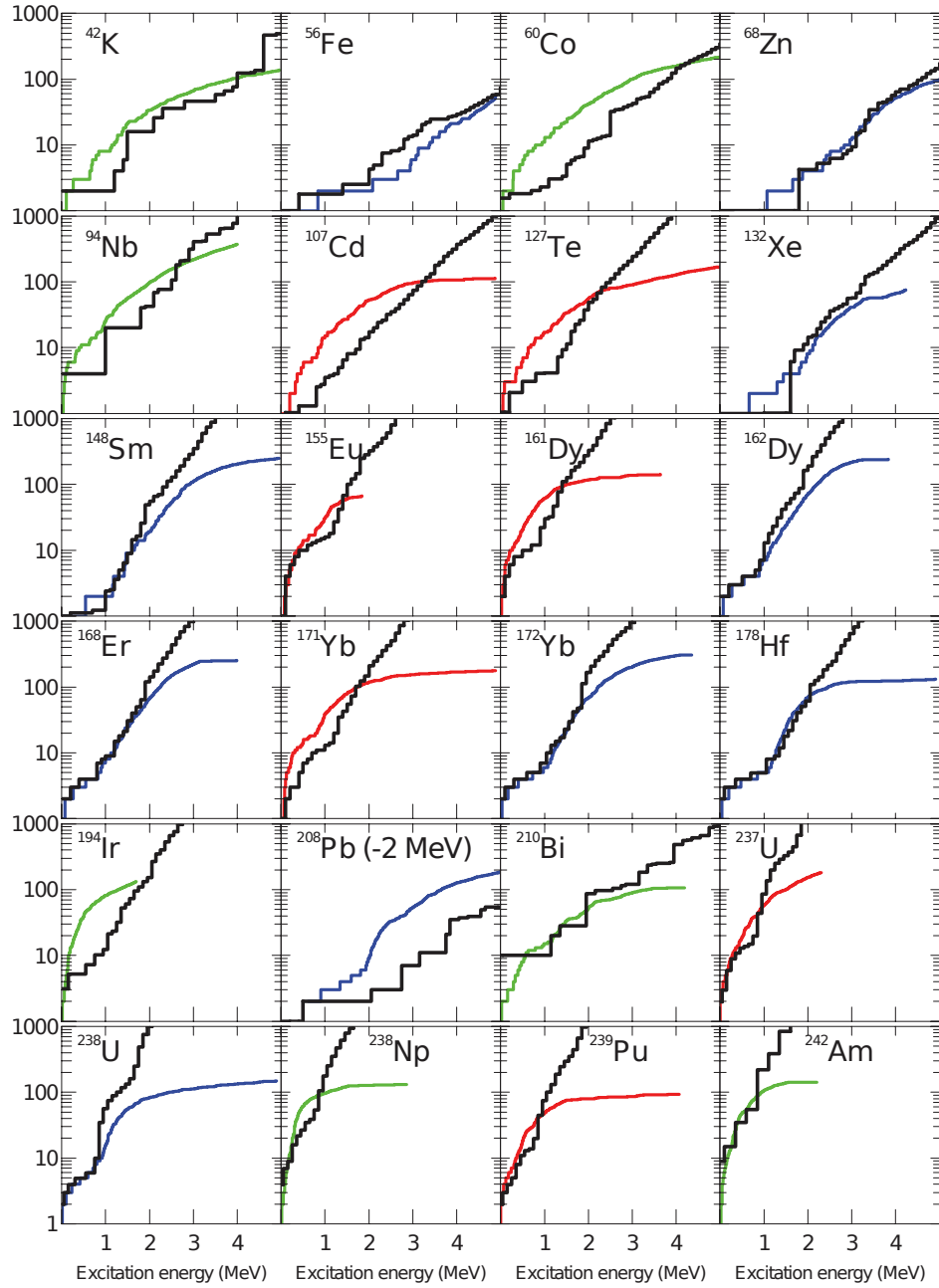


Figure 2: Comparison of the cumulative number of observed levels (colored lines) with the current combinatorial method (thick black line). Experimental data for even-even, odd-A, and odd-odd nuclei are shown by the blue, red, and green lines, respectively. Figure reproduced from Ref. [81].

for example

$$a_1^\dagger a_2^\dagger a_3 a_4 = \frac{1}{4} [(\hat{O}_{14} + \hat{O}_{23})^2 - (\hat{O}_{13} + \hat{O}_{24})^2] + \frac{1}{2} [\hat{O}_{14}, \hat{O}_{23}] - \delta_{24} \hat{O}_{13}. \quad (60)$$

This is the so-called density decomposition while it is also possible to use the pairing form working with the operators  $a^\dagger a^\dagger$  and  $aa$ . The pair operators in all cases carry correct quantum numbers of spin and isospin. It is not clear at this stage how it would be possible to include many-body interactions in this scheme except as perturbations.

The ensemble average of any observable can be written as [87]

$$\langle O \rangle_\beta = \frac{\langle \Psi | e^{-\beta H/2} \hat{O} e^{-\beta H/2} | \Psi \rangle}{\langle \Psi | e^{-\beta H} | \Psi \rangle}. \quad (61)$$

Here  $|\Psi\rangle$  is a trial wave function, for example a Slater determinant with the global quantum numbers of interest. The evolution with  $\beta \rightarrow \infty$  and the Hamiltonian  $H$ , would lead to the state of lowest energy at given symmetry. A possible way to the level density may go through the calculation of energy  $E(\beta)$ , statistical sum  $Z(\beta)$  and the inverse Laplace transformation [88].

## 4.2 Introducing auxiliary fields

The practical calculations use the *Hubbard-Stratonovich (HS)* transformation [89, 90], when the interval of  $\beta$  is subdivided into  $N_\beta$  small slices  $\Delta\beta = \beta/N_\beta$  and in each  $n^{\text{th}}$  interval a real auxiliary field  $\lambda_{jn}$  is introduced attached to the operator  $\hat{O}_j$  (we choose the notation  $\lambda$  instead of the traditional  $\sigma$  used above and below in different meanings). With the quadratic form of the actual many-body Hamiltonian including various operators  $\hat{O}_j$  of eq. (58),

$$h_n = \sum_j \{ \epsilon_j \hat{O}_j + p_j g_j \lambda_{jn} \hat{O}_j + (1/2) |g_j| \lambda_{jn}^2 \}, \quad (62)$$

one comes to the partition function  $Z(\beta)$ , eqs. (14,18). For each set of auxiliary fields  $\{\lambda\}$ , the contribution to  $Z(\beta)$  is of the Gaussian type describing the propagation of independent fermions in the presence of those external fields. The phase factor  $p_j$  comes from the HS transformation being equal to  $\pm 1$  for negative  $g_j$  and  $\pm i$  for positive  $g_j$ .

The total result is given [86] by the functional integral over auxiliary fields,

$$e^{-\Delta\beta H} = \int_{-\infty}^{\infty} \prod_j d\lambda_{jn} \sqrt{\frac{\Delta\beta |g_j|}{2\pi}} e^{-\Delta\beta \sum_j h_{jn}} \quad (63)$$

The output can be presented as  $[e^{-\Delta\beta H}]^{N_\beta}$ , or symbolically as the integral over auxiliary fields  $\int \mathcal{D}\lambda \mathcal{G}(\lambda) U(\lambda)$ , where the quadratic over  $\lambda$  parts of  $h_{jn}$  in eq. (63) give the Gaussian measure

$$\mathcal{G}(\lambda) = e^{-(1/2)\Delta\beta \sum_{jn} |g_j| \lambda_{jn}^2}, \quad (64)$$

while  $U(\lambda)$  is a one-body propagator for independent particles in the field  $\lambda$ .

In this way the real system of interacting particles is effectively reduced to a system of non-interacting particles independently propagating in time-dependent external fields. The use of auxiliary fields allows one to work with much larger orbital spaces. The resulting functional integrals over auxiliary fields are usually evaluated [86, 87] by the Monte-Carlo strategy, for example by some versions of the Metropolis method [91].

### 4.3 Shell-model Monte Carlo approach

The practical applications of this computationally involved approach use a positively defined weight function

$$W(\lambda) = \mathcal{G}(\lambda) |\zeta(\lambda)| \quad (65)$$

usually taken as a Gaussian (64). Here  $\zeta(\lambda)$  is the trace of the chronologically ordered (in imaginary time) evolution operator for a certain set of auxiliary fields. Finally, an expectation value of a physical observable  $\hat{Q}$  is given by the symbolic expression in terms of the normalized functional integral over those fields,

$$\langle \hat{Q} \rangle = \frac{\int \mathcal{D}\lambda W(\lambda) \langle \hat{Q} \rangle_\lambda \text{sign}\zeta(\lambda)}{\int \mathcal{D}\lambda W(\lambda) \text{sign}\zeta(\lambda)}, \quad (66)$$

calculated by the Monte Carlo sampling. The general line of calculations goes from the canonical thermal energy  $E(\beta)$  found as  $\langle H \rangle_\beta$  to the partition function  $Z(\beta)$  and the level density in the saddle-point approximation. The whole procedure, being more economical computationally compared to the full straightforward diagonalization, allows one to use bigger orbital spaces. However, for each temperature, a new Monte Carlo sampling is required.

Citing [92], *a potential problem in the Monte Carlo method is that the sign should be well determined*. Possible oscillations of the sign in eq. (66) from sample to sample lead to the large uncertainties in the functional integral. In many realistic cases this sign is fixed. The favorable situations include important multipole-multipole interactions of the multipolarity  $L$  with the sign  $(-)^L$  in even-even nuclei (or for even  $A$  and  $N = Z$ ). However, this is not the case, for example, in the use of the cranking model when the Hamiltonian includes an external rotation operator  $-\omega J_x$  that breaks time-reversal invariance, especially for large rotational angular velocity.

One practical recipe for overcoming the sign problem was suggested in [93]. All interaction operators are subdivided into “good” guaranteeing no sign problem (main collective interactions belong to this category) and “bad” ones. The force of a bad interaction acquires a variable parameter which first artificially makes the interaction good allowing the Monte Carlo calculation, and the results then are numerically extrapolated to the bad values. This worked well for the observables (quadrupole, magnetic and Gamow-Teller operators) in  $^{54}\text{Fe}$  although the character of interpolation to the good region is rather arbitrary.

The complete  $pf + g_{9/2}$  shell was treated with the Monte Carlo shell model in Ref. [54]. The two-body interaction suggested in Ref. [94] was used for calculations with the conclusion that this space should be sufficient for the description of the level density up to 20 MeV excitation energy. However, in order to be insensitive to the sign problem only a specially reconstructed part of the full Hamiltonian was practically used; another remaining problem was a presence of spurious center-of-mass excitations due to the  $g_{9/2}$  subshell included for description of the negative parity levels in  $^{56}\text{Fe}$ . Instead of exact spectroscopic information, the quadrupole strength function was calculated. A broader application of the same approach to nuclei from iron to germanium was made in Ref. [95], in a reasonable agreement with the compilation of data [96]. For a group of neighboring nuclei, including odd- $A$  and odd-odd ones, the calculations can be simplified by using a single “mother” nucleus and using the re-projection [97] to the actual particle number. The procedure is not fully reliable at relatively low energy.

The next development of the method was progressing in several directions. An attempt to generalize the approach to the continuum levels was undertaken in Ref. [98] based on the known relation between scattering phases and the single-particle resonance density [99]. This makes it possible to propagate the statistical properties of the single-particle spectrum and again apply

the shell model Monte Carlo approach. After continuing in this way the statistical properties of the single-particle spectrum and again apply the shell model Monte Carlo approach. At temperature up to 4 MeV in medium nuclei, the back-shifted Fermi-gas approach with phenomenologically adjusted parameters works better than at lower energies. This is where the continuum shell model in its various versions might be a good future development.

Based on the Monte Carlo method, one can also study the angular momentum coupling in the intrinsic frame of a deformed nucleus and the effective moment of inertia [100, 101] reproducing qualitatively known pairing reduction of the moment of inertia and corresponding even-odd effects. The application to heavy deformed nuclei, such as  $^{162}\text{Dy}$ , demonstrated the possibility to cover large orbital spaces necessary for the description of static deformation [102, 103], still with the limited interaction (pairing and multipole-multipole forces) and special approximate ways for finding the ground state energy. Applications to heavy deformed nuclei with their complex low-energy structure require special stabilization methods [105]. The comparison with the data is typically favorable (on a logarithmic scale) but it is hampered in many cases by the uncertainty in parity of excited states.

## 5 Quantum chaos and thermalization

### 5.1 Mesoscopic physics and quantum chaos

The atomic nucleus is a typical object of the mesoscopic world. The systems which belong to this world consist of a relatively small number of interacting quantum particles. In the nuclear case the system is bound by this interaction but in other examples, such as cold atoms in traps, the binding can be mainly provided by external fields. Among the inhabitants of this world we can mention complex atoms and molecules, including biological ones, atomic clusters, artificial condensed matter nano-devices etc. The future quantum computers also would belong to this class being constructed of individual quantum blocks. The number of interacting elements is usually large enough to create collective macroscopic features and statistical properties. On the other hand, the system is still sufficiently small in order to reveal individual quantum states which can be studied experimentally and theoretically. This richness of properties puts such systems on the frontiers of research and multiple applications.

The nucleus is self-bound. The binding is the result of the coherent interaction between the nucleons that creates the mean self-consistent field. Certainly, the mean field does not exhaust all capacities of the interaction. The remaining components of dynamics are responsible for the collective distortions of the mean field (rotational and vibrational as mentioned above) but also for many incoherent, roughly speaking collision-like, processes of particle interaction on the background of the mean field. In the case of quantum computers such interactions between the computational units (qubits) could be harmful converting a pure quantum state necessary for the binary code into a complicated many-body mixture. In many situations one has to stipulate for special measures suppressing the resonance interactions between the qubits [106].

In nuclei the influence of residual interactions goes in several directions changing significantly the density of states formed by the mean field. We have already mentioned the effects of collective enhancement, mainly due to the lowering of energy of numerous rotational and vibrational states built on top of simple particle, or quasiparticle, configurations. The simplest, and the most visible inevitable effect is the transformation of the pure mean-field, or paired BCS, states into very complicated superpositions. The genuine collective states made up a relatively small fraction of the spectrum, they are coherent superpositions of simple modes with certain quantum numbers, like low-lying quadrupole or octupole vibrations, giant multipole resonances, or collective rotations. Starting from some excitation energy, in reality after breaking a small number of pairs, the spectrum consists mainly of the big incoherent linear combinations of basis mean-field states. This happens unavoidably as the level density grows just by combinatorics and mixing of simple close in energy states becomes strong even with weak residual interactions. Then, if continuum effects are weak, the energy spectrum locally consists mostly of close states of quite similar complicated nature whose observable properties, such as expectation values or transition amplitudes of simple operators, are gradually changing as a function of energy.

The situation of the preceding paragraph is essentially a characteristic of what can be called “quantum chaos”. We will not discuss here a notorious question of relation between classical and quantum chaos. The standard spectral measures of quantum chaos [6, 7, 107] are usually *local*, for example the distribution of spacings between neighboring levels. Such characteristics in many cases require the “unfolding” of the spectrum when the energy spacings are expressed in the units of the local mean spacing. On the contrary,

we are interested in the evolution of observables, first of all the level density, along the spectrum. However, we will see that the chaotic nature of the majority of stationary states allows one to simplify the picture of the statistical level density.

## 5.2 Some measures of quantum chaos

The simplest signature of quantum chaotic dynamics is usually given in terms of the local level repulsion (49). If the incoherent interactions on top of the mean field are gradually switched on in a mesoscopic system, the simple basis states with the same values of exact constants of motion evolve through multiple avoided crossings. Already at a rather weak residual interaction, the system comes close to this stage of local level repulsion. More crossings are required to significantly mix the wave functions.

Using the mean-field basis of states  $|k\rangle$ , we express the wave function of a stationary state as

$$|\alpha\rangle = \sum_k C_k^\alpha |k\rangle, \quad \sum_k |C_k^\alpha|^2 = 1. \quad (67)$$

The complexity of a state  $|\alpha\rangle$  can be estimated through the amplitudes  $C_k^\alpha$ . If there are  $\mathcal{N}^\alpha \gg 1$  significant amplitudes, the normalization of the state vector defines their typical small magnitude  $|C_k^\alpha|^2 \sim 1/\mathcal{N}^\alpha$ . We have to stress here that this is the *relative* complexity of a given stationary state  $|\alpha\rangle$  with respect to the chosen basis  $|k\rangle$ . In fact, this carries some advantage: one can measure the relations between different bases. The choice of the reference basis as that of the mean field approximation assumes that the mean field basis concentrates the regular features of the inter-particle dynamics while the interactions that on average do not contribute to the mean field are random or irregular.

The exception can be a collective mode, like a shape vibration or giant resonance, when the excitation is built of many *coherent* contributions of various simple modes. In this case many amplitudes  $C_k^\alpha$  have coherent phases. Except for the states of the lowest energy, such excitations are usually not stationary states but superpositions of many genuine stationary components close in energy (a microscopic analog of damping [108]). A collective state  $|\alpha\rangle$  can be recognized [109] by the so-called *phase correlator*,

$$P^\alpha = \frac{1}{\mathcal{N}^\alpha} \sum_{kk'}^{\mathcal{N}^\alpha} C_k^\alpha C_{k'}^{\alpha*}, \quad (68)$$

that can have a value of the order one only if many components have coherent phases. All typical states have a small value of this quantity.

There are several convenient measures of the degree of complexity of eigenstates. The *correlational (Shannon) entropy* of a certain stationary state  $|\alpha\rangle$  is defined as

$$S^\alpha = - \sum_k |C_k^\alpha|^2 \ln |C_k^\alpha|^2. \quad (69)$$

A similar characteristic is the inverse second moment of the distribution of amplitudes, or *inverse participation ratio* that gives the effective number of principal components (NPC),

$$(\text{NPC})^\alpha = \left[ \sum_k |C_k^\alpha|^4 \right]^{-1}. \quad (70)$$

These measures, in distinction to (68), are insensitive to the phases of the component.

The mathematical limit of quantum chaos is given, for systems with interactions invariant under time reversal, by the *Gaussian orthogonal ensemble* [5, 6, 107]. This is an ensemble of Hermitian matrices with uncorrelated matrix elements and Gaussian distribution of probability determined by the trace of the squared Hamiltonian. In the limit of a large dimension  $\mathcal{N}$ , the average over the ensemble value of the correlational entropy (69) equals  $\ln(0.48\mathcal{N})$  while the effective number of principal components is  $\mathcal{N}/3$ . This is the limit of full delocalization of the eigenvectors over entire basis space. In realistic many-body systems, the states are characterized by the parameter equivalent to  $\mathcal{N}$  which is smaller than the total dimension but still large,  $\mathcal{N} \gg 1$ , and smoothly changing along the spectrum.

Nuclear physics provides examples of spectra very close to the GOE predictions [110, 111, 112]. This happens in spite of the fact that the nuclear Hamiltonians used in realistic shell-model calculations do not have exact Gaussian orthogonal ensemble (GOE) properties. The practical two-body interactions lead to the matrices in the mean-field basis which are not random (all two-body collisions have the same matrix elements for several possible spectator configurations on the orbitals not participating in a given process). The matrices are also quite rarefied due to the conservation laws. This similarity to the GOE leads to the impression that the qualitative features of quantum chaos are very generic being almost universal for realistic

many-body systems with strong interaction, almost independent of actual statistics of the Hamiltonian matrix.

One important manifestation of chaotic dynamics is the enhancement of weak interactions. As simple estimates show [113], the matrix elements of observables between two chaotic states of the similar degree of complexity are small,  $\propto 1/\sqrt{\mathcal{N}}$ . But the spacings between the states mixed by such operators are typically small,  $\propto 1/\mathcal{N}$ , and the effects of perturbative mixing are enhanced in average  $\propto \sqrt{\mathcal{N}}$ . First of all, this is empirically seen in the striking enhancement of parity mixing between  $s$ - and  $p$ -neutron resonances seen through the polarized neutron scattering off spherical nuclei [114, 115, 116, 117]. Here the additional dynamical factor present due to the large ratio of the widths of  $s$ -resonances compared to those of  $p$ -resonances leads to the parity violation effects up to 10% (the original estimate without chaotic enhancement would be  $10^{-7} - 10^{-8}$ ). A big enhancement (but without the dynamical factor) is also seen in the neutron-induced fission [118, 119, 120, 121]. The parity-violating fragment asymmetry turns out to be independent of the mass or kinetic energy distribution. Final distributions of global observables are formed at later stages of the fission process while the parity violation occurs earlier, in the “hot” compound nucleus with chaotic enhancement of weak perturbations, being preserved after that.

### 5.3 Thermalization

The detailed “microscopic” view of the spectrum and the analysis of the spacing distributions between the levels of the same symmetry class, being important steps for seeing the onset of chaos, do not help in the problem of the global level density as a function of energy and other exact constants of motion. But the conclusion that the generic stationary wave functions are complicated “chaotic” superpositions of many simple basis functions leads to the obvious analogies to statistical thermodynamics. Here we do not have any thermostat (heat bath) that establishes a certain temperature inside the system coupled to the thermostat. Nevertheless, as in standard statistical mechanics, we have the smooth evolution of observables and degree of complexity along the spectrum. The measures of complexity, such as (69) and (70), turn out to be smooth functions of excitation energy [110, 122, 112] depicted as a narrow band with small fluctuations within the band diminishing with the growth of the dimension. In this sense such measures become *thermodynamic functions*.

The process of thermalization in closed finite systems of interacting constituents was reviewed recently [123] with numerous examples of atomic, nuclear and spin systems revealing the signatures of thermal equilibrium without an external heat bath. More mathematically oriented review can be found in [124]. To characterize this equilibrium it is usually sufficient to analyze a typical stationary wave function studying its complexity, mean values, and fluctuations of observables. This is an essence of the so-called *eigenstate thermalization hypothesis* (ETH) intensely discussed recently [125, 126, 127]. It is less known that the equivalent statement was formulated much earlier in the *Statistical Physics* volume by Landau and Lifshitz [19]. In fact, this idea is a continuation of the line going back to Boltzmann (*molecular chaos*), Russian physicist N. Krylov [128] and Van Hove [129].

There are several quantitative measures which can be used to describe the process of thermalization in a small system. The level density gives rise to the partition function and corresponding free energy and thermodynamic entropy of the system as a whole. The good illustrations come from nuclear [110], atomic [130], and condensed matter analysis, see [123] and references therein, where the exact diagonalization of the quantum Hamiltonians was presented. Of course, such examples, as a rule, refer to a limited orbital space and therefore can describe the real level density only up to a certain excitation energy. In this finite space the level density is given by a bell-shape curve with the maximum  $E_m$  in the middle of the spectrum. The shape of the curve is close to Gaussian, and its width  $\sigma$  allows one to define the temperature,

$$T(E) = \frac{\sigma^2}{E_m - E}. \quad (71)$$

The symmetry of the curve relies on the particle-hole symmetry of the dynamics; the right half,  $E > E_m$ , corresponds to negative temperatures (prevailing occupation of highly excited levels). The transition between the two branches goes through formally infinite temperature when all quantum states are populated equally; this feature is clearly seen if the dimension of the space is large enough [110].

To characterize thermal equilibrium one can apply various measures - *thermometers*. It is natural to look at the particle distribution over single-particle levels. If one has a full solution for a quantum system, it is possible to analyze each stationary state and find the mean occupancies of all single-particle orbitals. It turns out that the distribution of nucleons in a complex

nucleus [110], as well as that of electrons in a complex atom [130, 131], is well described by the standard Fermi-Dirac statistics with the parameters of temperature and chemical potential smoothly changing along the excitation energy. The resulting evolution of the temperature parameter extracted from individual states well agrees with the global description (71). It is important to note that such an agreement occurs only if the interaction strength is in compliance with the choice of the mean field which creates the orbitals [110]. Too weak or too strong residual interaction destroys this correspondence so that the single-particle thermometer stops working properly. We notice that the shell-model (configuration interaction) approaches allow one to study, through variation of the parameters, the dependence of physical characteristics on various parts of the Hamiltonian. This is quite useful for creating a more complete physical picture.

## 6 Shell model level density

### 6.1 Briefly about the nuclear shell model

Here we use the term "shell model" in a broad sense including various formulations. The model is defined by the orbital space and the Hamiltonian that consists of single-particle orbitals and residual interactions. The orbital space can include an inert core plus valence orbitals or start *ab initio* without a core. Some formulations are still practically limited to rather light nuclei and nuclei around the closed shells. The forces may include many-body interactions or be restricted to a two-body level. Anyway, one constructs the Hamiltonian matrix and tries to diagonalize it, exactly or through some approximations. Currently the exact diagonalization has a limiting dimension of approximately  $10^{10}$ . Of course, the full diagonalization in a finite Hilbert space can provide the physically reliable level density only up to some excitation energy where the states outside the original space enter the spectrum. There are also limitations in quantum numbers of stationary states (for example, parity or total spin) as the choice of the corresponding classes of states may be distorted by the truncation of the space.

As an example with a rich history of many successful applications let us characterize the well developed shell model for the *sd*-nuclei. This family of nuclides covers the isotopes from  $^{16}\text{O}$  to  $^{40}\text{Ca}$ . The model includes the spherical orbitals  $0d_{5/2}$ ,  $1s_{1/2}$ , and  $0d_{3/2}$  with their ordering and positions

determined by the realistic spin-orbit splitting. Here only the states of positive parity are possible which could be a rather good approximation to real nuclei up to energy of about 10-12 MeV. If we limit ourselves by two-body forces respecting the isospin invariance, the most general interaction Hamiltonian contains 63 independent matrix elements. The most rich subspaces of states with a given total spin  $J$  have a dimension of the order of few thousand. Of course, the complete diagonalization is possible and the results of the full spectrum of stationary states and transition rates were discussed in many publications, for example the case of  $^{28}\text{Si}$  was analyzed in detail in Ref. [110]. The full knowledge of this model allows for its use as a touchstone for various physical assumptions.

A serious advantage of the shell-model approach is in the possibility to study the physical influence of individual parts of the Hamiltonian by applying the variation of certain matrix elements or their groups selected in a certain way. For example, the old question of the predominance of prolate deformation in the ground states on non-spherical nuclei [134] was clarified indicating that the main role here is played by the interaction acts changing the orbital momentum of one of the colliding particles by  $\Delta\ell = 2$ . We will also later use a similar approach studying the influence of individual parts of the residual interactions on the level density parameters. In practice, often not all interaction matrix elements are precisely fixed by the low-energy observables. Some matrix elements are still not reliably defined, especially if the corresponding processes weakly change the collective properties of the mean field and low-lying dynamics. In general, many such contributions are those which were mentioned earlier as responsible for the incoherent collision-like processes. As we will see, these parts of the interaction are important for certain features of the level density.

The mentioned above case of  $^{28}\text{Si}$ , or the similar consideration of  $^{24}\text{Mg}$  ([68], Chapters 20 and 25), show that the exact shell model solution, as a rule, provides the smooth Gaussian type of the level density while typical attempts to limit the Hamiltonian by the mean field parts (maybe plus pairing in the BCS or HFB form) create the level density that displays noticeable oscillations reflecting the subshell structure. This is a typical manifestation of the role of the “collision-like” parts of the effective interaction which really lead to the chaotization of the dynamics.

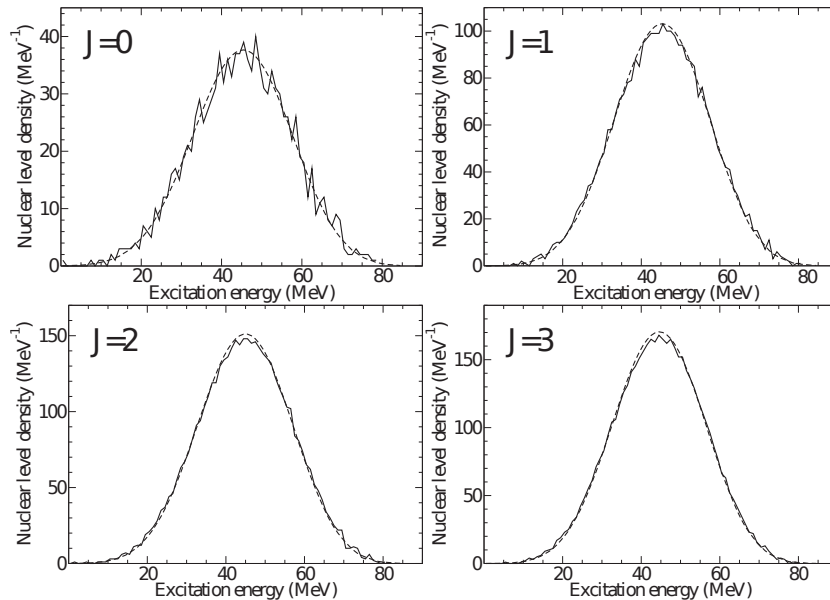


Figure 3: Nuclear level densities for  $^{24}\text{Mg}$ , positive parity and various spins, for the  $sd$ -shell and USDB two-body interaction (taken from Ref. [152]); full shell-model diagonalization (solid curves) vs moments method (dashed curves).

## 6.2 Moments method

As mentioned above, the interaction between the constituents in a closed mesoscopic system is responsible for quantum chaos. The combinatorial growth of the level density, irrespectively of its details, leads to unavoidable strong mixing of simple mean-field excited states and formation of the complicated stationary combinations. In contrast to the local measures of this chaotic mixing, such as the unfolded level spacing distribution and its fluctuations, we are interested in a global behavior of the level density. As this scenario arises from very general characteristics of mesoscopic objects, one can expect certain typical statistical regularities of the level density. In a sense, the process of chaotization, or stochastization, of the dynamics is so common that there should exist a general statistical approach to its calculation for a given Hamiltonian.

This idea, along with a practical method of calculating the level densities, was formulated by French and collaborators [137] and systematized in

the book by Wong [138], see also the extensive compilation of related papers in [139]. Essentially, the method is based on the central limit theorem and the partition structure of the mean-field picture (in the first applications, the level density was presented as a sum of non-interacting level densities empirically convoluted with Gaussians). As a function of excitation energy, the resulting level density in a finite Hilbert space of interacting particles is close to Gaussian as seen in the shell-model examples. Of course, the whole approach called *statistical spectroscopy* has much more applications not limited by the level density. In particular, one can find typical distributions of matrix elements and transition rates very important for practitioners [7]. It can be also generalized for the physics of resonances and reactions in the continuum [140, 141].

In practice, the moments method reduces to the calculation of traces of the powers of the Hamiltonian avoiding the full diagonalization. The working algorithm was gradually improved in successive publications [142, 144, 145]. It was made available in the open access with the computational details given in [146].

To start with, we have at our disposal the mean field, single-particle orbitals (usually  $j$ -levels), and a number of neutrons and protons populating them in accordance with the Pauli principle. Each allowed configuration given by the distribution of nucleons over the orbitals is called a *partition*. The general two-body interaction can be written as

$$H = \sum_1 \epsilon_1 a_1^\dagger a_1 + \frac{1}{4} \sum_{1234} V_{12;34} a_1^\dagger a_2^\dagger a_4 a_3, \quad (72)$$

where the single-particle quantum numbers  $1, \dots$  labeled here by numerals include the radial index, level spin  $j$ , its projection  $m$  (energies  $\epsilon_1$  do not depend on projections) and isospin projection  $\tau$ ; the antisymmetrized binary interaction matrix elements satisfy the angular momentum conservation. Let  $\alpha$  denote a complete set of global characteristics for a many-body nuclear state: neutron and proton numbers, total spin  $J$ , parity  $\Pi$ , isospin  $T$ . Within a given partition  $p$ , one can construct  $D_{\alpha p}$  states of this class and calculate the energy centroid of the many-body states in the class  $\alpha$  generated inside this partition,

$$E_{\alpha p} = \langle H_{\alpha p} \rangle \equiv \frac{1}{D_{\alpha p}} \text{Tr}^{(\alpha p)}(H), \quad (73)$$

This trace includes mean-field energies of the orbitals occupied in the partition  $p$  and matrix elements of the interactions diagonal with respect to the

occupancies of the levels fixed in the definition of the partition. This is the *first moment* of the Hamiltonian (72).

The *second moment* being defined similarly to (73),

$$\langle H_{\alpha p}^2 \rangle \equiv \frac{1}{D_{\alpha p}} \text{Tr}^{(\alpha p)}(H^2), \quad (74)$$

includes the bilinear combinations of mean-field energies and interaction matrix elements forming the two-step processes within the partition  $p$  with the inclusion of transitions to the configurations outside this partition, see the detailed structure in [146]. It might be practically convenient to work with the  $M$ -basis avoiding the procedure of forming exact angular momentum multiplets and corresponding  $3nj$ -algebra. Also the neutron-proton formalism may be applied instead of the full isospin description. With the Hamiltonian conserving total spin and isospin, all exact symmetries are respected.

It is known for a long time [107, 110] that the level density inside a partition is rapidly converging to the Gaussian. Additional interactions contribute in quadratures to the resulting width. The first two moments, (73) and (74), allow to construct the Gaussian distribution  $G_{\alpha p}$  for a given partition. It has a centroid

$$E_{\alpha p} = \langle H_{\alpha p} \rangle, \quad (75)$$

and the width  $\sigma_{\alpha p}$ ,

$$\sigma_{\alpha p}^2 = \langle H_{\alpha p}^2 \rangle - \langle H_{\alpha p} \rangle^2. \quad (76)$$

It is also possible [138] to construct higher moments expressed in terms of corresponding traces. However, the comparison of the approximation based on the two lowest moments with exact shell-model calculations shows that it is not necessary, especially if these moments are improved by the following. We modify the functions  $G_{\alpha p}$  introducing [142] the *finite range Gaussians*  $G_{\eta}(x, \sigma)$  where the tails are cut off at a distance  $\pm\eta\sigma$  from the centroid. The parameter  $\eta$  is typically between 2.5 and 3 which is confirmed by the analysis of the strength functions found [143] in the shell model with the same Hamiltonian. The finite range Gaussian has to be correspondingly renormalized. In this way we come to the functions

$$G_{\alpha p}(E) = G_{\eta}(x = E - (E_{\alpha p} - E_{\text{g.s.}}), \sigma_{\alpha p}), \quad (77)$$

which determine the effective contribution of a given partition  $p$  to the level density in the class of states  $\alpha$ ,

$$\rho_{\alpha}(E) = \sum_p D_{\alpha p} G_{\alpha p}(E). \quad (78)$$

The ground state energy  $E_{g.s.}$  entering eq. (77) should be determined separately, either by the exact shell-model solution, or using other ways, such as exponential convergence [142, 147, 148], or just by a special fit.

An important addition to the method is in handling the cases for the orbital space that includes several main shells. Between the oscillator shells of opposite parity there are, among possible excitations, the fictitious ones corresponding to the quanta describing the center-of-mass excitation. These excitations are to be removed from the full shell-model level density. In the shell model and in Monte Carlo approaches this is sometimes done by the artificial shift of the center-of-mass excitations to sufficiently high energy. Here one can use [145] the set of recurrence relations [149, 150, 151] taking away possible unphysical admixtures. The computational procedures and the perspectives of parallelization are discussed in [146].

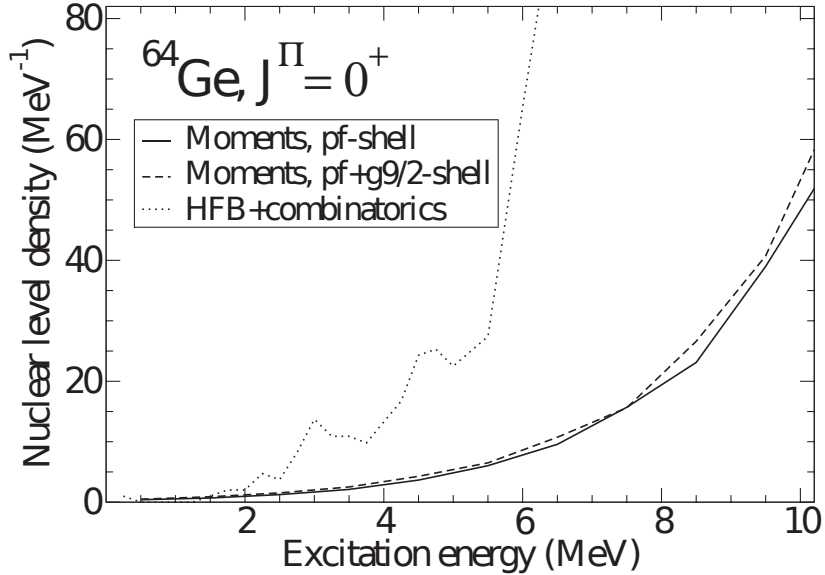


Figure 4: Low-energy level density for  $^{64}\text{Ge}$ , spin  $J = 0$  and parity  $\Pi = +1$ . The solid curve presents the calculation in the  $pf$  shell with the GXPF1A interaction, the dashed curve corresponds to the calculation in the larger model space with the level  $g_{9/2}$  added, and the dotted curve presents the results obtained using the HFB single-particle energies and the combinatorial method [47]. Taken from Ref. [152].

### 6.3 Applications

Any new approximate method has to be tested in comparison with the exact solutions if the latter are available. Figure 3 shows the level density calculated for the  $^{24}\text{Mg}$  nucleus in the framework of exact diagonalization using the two-body USDB interaction [153] and with the moments method [152] applying the same input (mean-field levels and two-body interaction). The moments method reliably reproduces the whole bell-shape curve of the level density as a function of excitation energy for different classes of states. Some small fluctuations are slightly smoothed compared to the exact solution, especially in the low-dimensional classes of states. There is also a minor deficit of states at the top of the Gaussian which could be corrected by adding the fourth moment. However, we have to recall again that the whole shell-model approach becomes much earlier just a model rather than the description of nature because of the admixture of configurations outside the included orbital space. In the physical region of excitation energy below 20-25 MeV the agreement between the moments method and shell-model diagonalization is very good.

In heavier nuclei, the shell-model approaches are expected to work reliably in a smaller interval of energies. Figure 4 shows the results for the  $J^\pi = 0^+$  states in  $^{64}\text{Ge}$  with the GXPF1A interaction. Below excitation energy of 10 MeV, the two versions of the moments method, just using the  $pf$ -shell, or adding the intruder  $g_{9/2}$  level and new matrix elements with elimination of spurious center-of-mass excitations, practically coincide. Intruder states become essential after excitation energy of 8-10 MeV. An example is shown in Figure 3 of Ref. [152]. At the same time, the results obtained [154] with the help of the HFB approach and the combinatorial method, show a significantly different behavior with large bumps and higher level density. The situation is very similar for other nuclei, for example  $^{52}\text{Cr}$  and  $^{54}\text{Fe}$ , as shown in [145].

Our level densities are describing fairly well the existing data. For example, Figure 5 shows the results of the moments method for  $^{52}\text{Cr}$  at neutron separation energy compared with other methods and  $p$ -wave RIPL data [70]. One needs to add contributions from all relevant  $J$  that can be built with  $p$ -wave neutrons, i.e.  $J = 2^+, 3^+, 4^+, 5^+$ .

The level densities are main inputs to reaction codes that calculate cross sections and reaction rates of interest for nuclear astrophysics. In the past

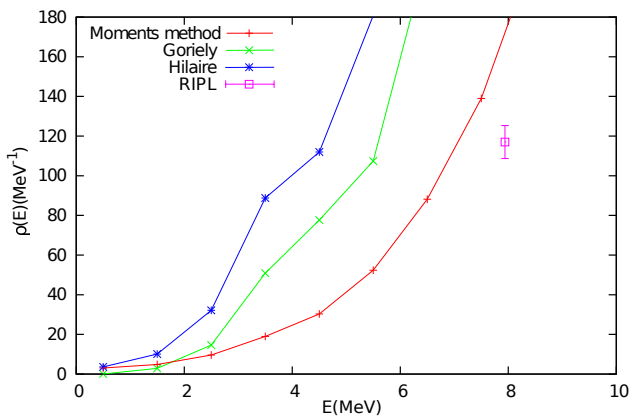


Figure 5: Comparisons for nuclear levels of  $^{52}\text{Cr}$  at neutron separation energy using different models: RIPL experimental data [70] vs moments method, and the results of combinatorial method provided in TALYS’ Goriely and Hillaire tables [172].

we used our tables of spin- and parity-dependent level densities [171] as input to the TALYS code [172] by replacing some tables in the code. This approach has two drawbacks: (i) the shell model level densities have a finite excitation energy range ( $< 12$  MeV), and an algorithm for continuation to higher excitation energy is needed, and (ii) changing tables is a complex process prone to errors. The TALYS code is already implementing the constant temperature model with the parameters extracted from the limited existing experimental data.

Using this approach we applied TALYS to calculate the differential cross section at backward angles for the  $^{58}\text{Fe}(^3\text{He},p)^{60}\text{Co}$  reaction studied experimentally by the Ohio group [173]. Figure 6 shows the results of our calculations (NLD-Moments) compared with the experimental data and the results obtained using Hillaire’s tables (model MD5 in TALYS). One can see that our level densities describe reasonably well the data and show a small improvement with respect to the MD5 results. As already mentioned, the approach used here is taking the MD5 level densities at excitation energies higher than 12 MeV that may be important due to the  $Q$ -values involved in the reaction. We plan to use the level densities of the moments method to extract the parameters for the constant temperature description, thus extrapolating the level densities to higher excitation energies. The further improvement should come from a better description of the reaction mechanism.

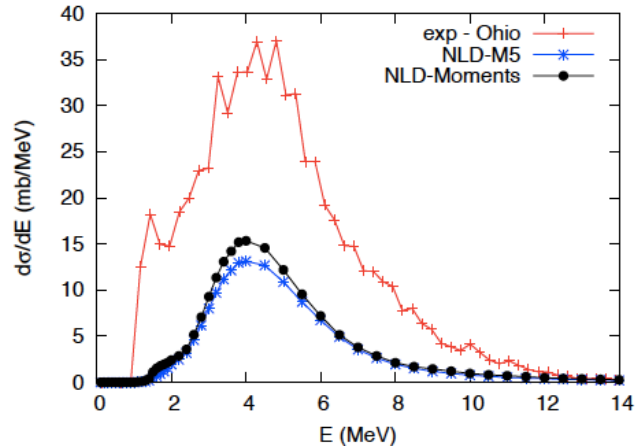


Figure 6: Comparison of the Hauser-Feshbach cross section for the  $^{58}\text{Fe}(^3\text{He},p)^{60}\text{Co}$  reaction using the level density given by the moments method and by Hillaire’s tables. The horizontal axis shows energy of the outgoing proton.

## 6.4 Role of various interaction components

The shell model, with its wealth of interaction matrix elements, allows one to study their specific roles in the formation of the final level density. For this purpose it is reasonable to divide the mean-field part and the residual interactions into groups supposedly responsible for the certain features of the resulting spectrum. Introducing a random element in the Hamiltonian and looking at the evolution of the density matrix of a given state in the presence of this perturbation [155] one can locate possible phase transitions in nuclear structure. In the same way it is possible to study the dependence of the level density on various parts of the Hamiltonian. As was already mentioned, the similar studies in the past [134] gave some evidence of the special role of the matrix elements changing the orbital momentum of one of the interacting particles by  $\Delta\ell = \pm 2$  in the formation of the deformed mean field.

The obvious coherent effect comes from pairing. It is known that the pairing interaction considered exactly, rather than in the BCS or HFB approximation, leads also to some chaotic features in the excited states of the system [109, 155, 156]. However, this “randomness” is not sufficient for full chaotization. It is natural that various independent components of interaction contribute individual mean square terms to the total level density;

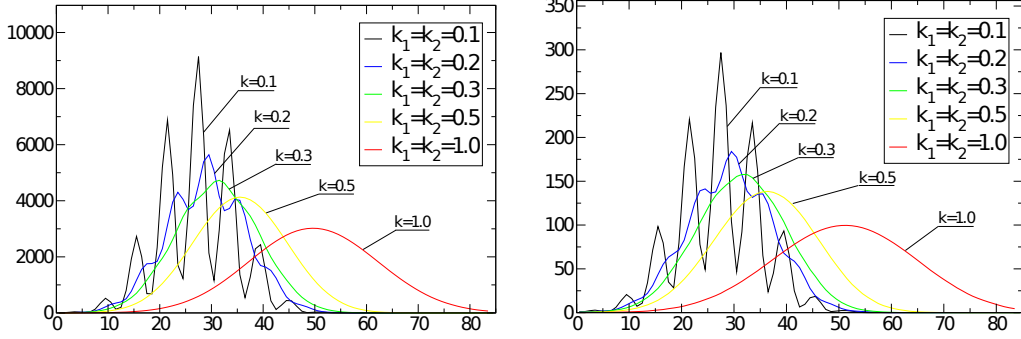


Figure 7: Level density for  $^{28}\text{Si}$  in  $sd$  model space. Different curves correspond to different scale factors,  $k = k_1 = k_2 = 0.1, 0.2, 0.3, 0.5, 1.0$  when the pairing and non-pairing parts of the interaction scale similarly. The left graph corresponds to the total density with all  $J$  included, while the right graph describes the evolution of the  $J = 0$  density.

neglecting them we would come to a narrow level density  $\rho$ . One can present the shell model Hamiltonian as a sum

$$H = h + k_1 V(\text{pairing}) + k_2 V(\text{non - pairing}) \quad (79)$$

and study the evolution of observables as a function of the parameters  $k_1$  and  $k_2$ . Here  $V(\text{pairing})$  includes only the matrix elements having the pairs  $J = 0$  with isospin 1 before and after the interaction. In the  $sd$  shell there are only six such matrix elements. The part  $V(\text{nonpairing})$  contains all remaining two-body matrix elements.

In Figure 7, the parameters  $k_1 = k_2$  are changed simultaneously from 0.1 to a regular value of 1 for  $^{28}\text{Si}$ , showing the full level density in the left part and partial level density in the subspace of total spin  $J = 0$  in the right part. The picture is typical for all classes of states: sharp peaks reflecting the subshell structure of the available space first combine into a unified indented wall and, with the further increase of the interaction, gradually form a more broad smooth bell-shape curve. The study the influence of each group of interactions, is further investigated in Ref. [152] where the set of level densities found by the exact solution for pure pairing when all interactions except for six matrix elements of pairing ( $J = 0$ , isospin 1) are excluded is shown. When the pairing strength factor  $k_1 < 1$ , the level density consists of several non-overlapping peaks corresponding to various excitations of the paired state (see e.g. Fig. 5 of Ref. [152]). Only for artificially enhanced

pairing,  $k_1 > 1$ , the level density becomes a bell-shaped curve in a function of excitation energy, still much more narrow than in the shell-model solution with the actual set of all interactions. The complementary evolution (normal pairing and increasing non-pairing strength) is illustrated by Figure 8. We conclude that both parts of the interaction in our crude subdivision (79) are important for the realistic result. Currently only approaches based on the shell model are capable of taking this into consideration.

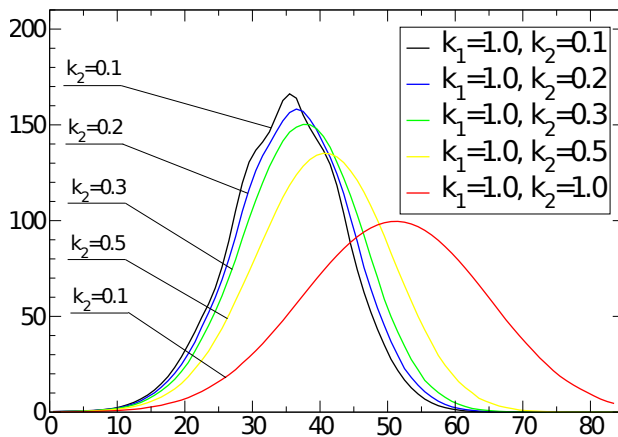


Figure 8: Level density for  $^{28}\text{Si}$ ,  $J = 0$ ,  $sd$  model space. The black curve presents  $k_1 = 1.0$ ,  $k_2 = 0.1$ , then the remaining parts of the interaction are increased together with  $k_2$  up to the red curve ( $k_1 = k_2 = 1.0$ ) that describes the realistic interaction. Taken from [152].

## 6.5 Comparison with Fermi-gas models

Using the Fermi-gas predictions (34) one expects the level density (summed over all classes of states) to be approximately described by

$$\ln[\rho(E)] + \frac{5}{4} \ln E = \text{constant} + 2\sqrt{aE}. \quad (80)$$

The slope of this line as a function of  $\sqrt{E}$  predicts the value of the main parameter  $a$ . The values extracted from the shell model are noticeably smaller than those found empirically from known low-lying levels [66] and especially from neutron resonances [157]. If we still have in mind the origin of the

parameter  $a$  as characterizing, eq. (31), the single-particle level density at the Fermi surface, it should be correlated with the filling of nuclear shells (mentioned above Rosenzweig effect [34, 35]). Indeed, one can qualitatively see the maxima of the found value of  $a$  in the middle of the shell. However, the big discrepancies between the data from the two sources indicate that the literally understood Fermi-gas description is not quite satisfactory. In the shell model the result of using eq. (80) also significantly depends on the energy range of fitting, Figure 9. The need for empirical higher values of the parameter  $a$  may reflect the fact that the realistic level density grows, as in the CTM approach, faster than in the Fermi-gas description.

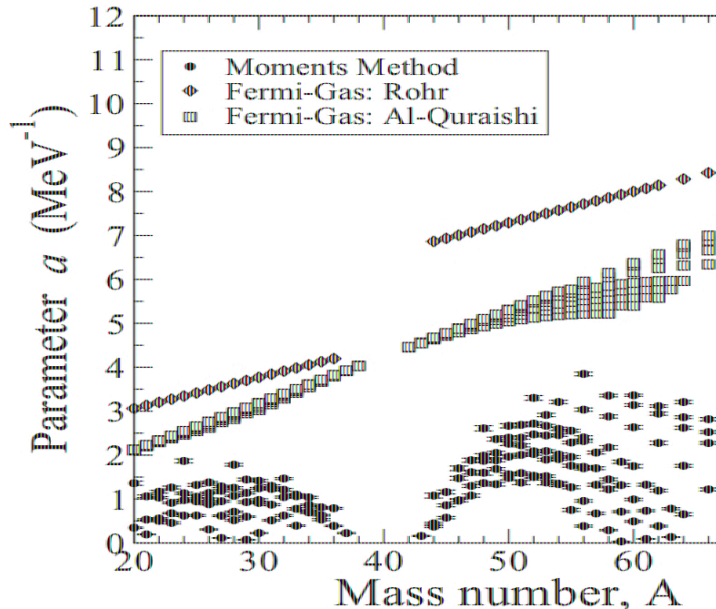


Figure 9: Interpolation of the single-particle level density parameter  $a$  with a fitting energy range 5-25 MeV: moments-method calculation with interpolation (black circles), fit using the experimental data on neutron resonances (Ref. [157], red diamonds), and fit using experimental low-lying levels (Ref. [66], yellow squares). Figure adapted from Ref. [152].

Using the back-shifted Fermi-gas description brings in an additional parameter of the shift that should not exactly coincide with the pairing gap or odd-even mass difference. As shown in [152], this may change the value of

the extracted parameter  $a$  by few percent only.

## 6.6 Spin cutoff parameter

Many applications require the knowledge of partial level densities for special classes of states, first of all for certain values of the total spin  $J$ . As shown in subsection 2.6, the assumption of random coupling of individual nucleon spins leads to the Gaussian distribution of partial level densities with the spin cutoff parameter  $\sigma_M$  defined, eq. (43), by the quantum numbers of available particle orbitals. The level density for a given value of  $J$  is then restored by the identity (1).

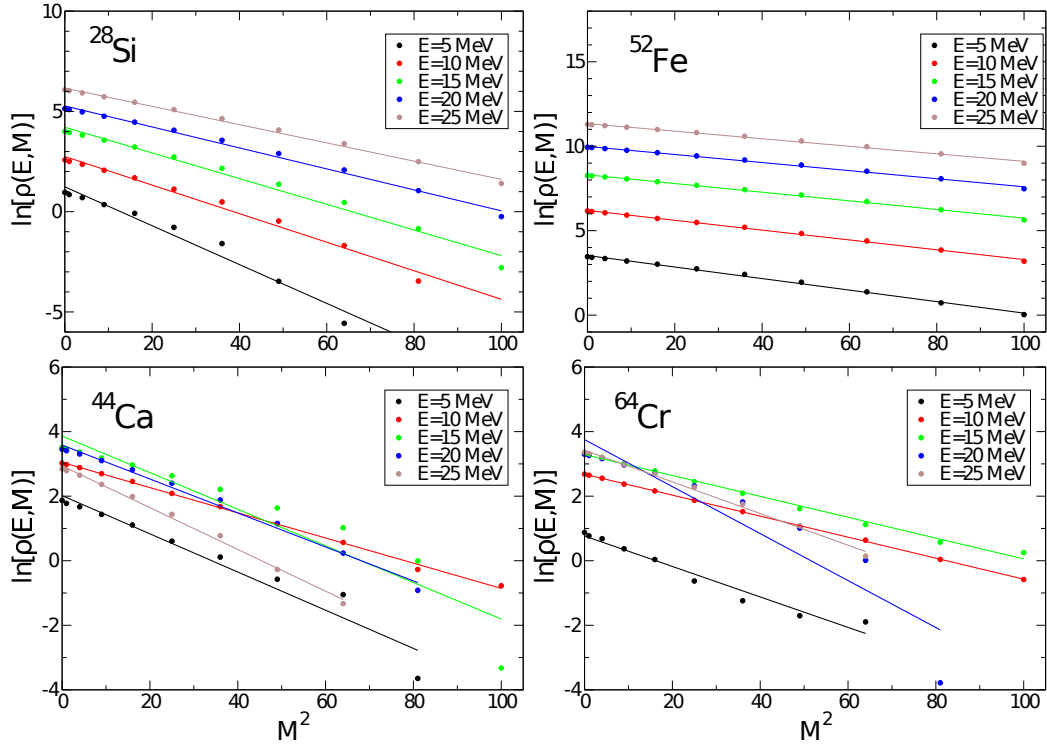


Figure 10: Logarithm of level density,  $\ln[(E, M)]$ , versus  $M^2$ , calculated for  $^{28}\text{Si}$ ,  $^{52}\text{Fe}$ ,  $^{44}\text{Ca}$ , and  $^{64}\text{Cr}$ . Different colors present different excitation energies: 5 MeV (black), 10 MeV (red), 15 MeV (green), 20 MeV (blue), and 25 MeV (brown). Dots correspond to the moments method calculations, the solid lines are linear interpolations (taken from [152]).

Such an assumption leads to the prediction that the level density as a function of the total angular momentum projection  $M$  satisfies

$$\ln[\rho(E, M)] = \ln[\rho(E, M = 0)] - \frac{M^2}{2\sigma_m^2}. \quad (81)$$

Here the spin cutoff parameter  $\sigma_m$  in general depends on energy. The main consequence of eq. (81) is the linear  $M^2$ -dependence of  $\ln \rho(E, M)$  easily verifiable by the shell-model results. Figure 10 illustrates the behavior of this logarithm for different nuclei; indeed, in many cases, see here examples of  $^{28}\text{Si}$  and  $^{52}\text{Fe}$ , it goes down linearly as a function of  $M^2$  with the monotonous parallel lifting of the line as a function of energy. This can be understood as a confirmation of the original idea of random spin coupling.

There are also exceptional cases, such as  $^{44}\text{Ca}$  and  $^{64}\text{Cr}$ , where the situation is more involved and there is no clearly determined parameter  $\sigma_m$ . The notion of random spin coupling does not work here well due to the isospin limitations in the shell-model description. The  $^{44}\text{Ca}$  nucleus has in this formulation only four valence  $f_{7/2}$  neutrons and the two-body interaction contains only matrix elements with the isospin of the pair equal to 1 so that many total spin values are impossible. Similarly, there are only four valence protons in the model for  $^{64}_{24}\text{Cr}_{40}$ . In such cases the prediction of random spin coupling can break down. The details of the energy behavior should be studied more carefully as they reflect shell effects and the evolution of the average moment of inertia from the superfluid to rigid-body rotation.

## 6.7 Collective enhancement revisited

In subsection 3.3 we briefly discussed the idea that low-lying collective states, vibrational and rotational bands increase the level density at low energy compared to the single-particle counting in Fermi-gas or mean-field models [36]. It is known that with the shell-model interaction Hamiltonian, in a sufficiently broad orbital space, one can describe the collective excitations and the shape transition to deformation. The exact operator equations of motion contain phonon excitations and correct rotational dynamics without artificial cranking and with the correct superfluid moment of inertia [38, 39]. Even with random interactions, collective states appear with a noticeable probability [134]. The existence of the collective enhancement is confirmed

with calculations along the chain of samarium isotopes with the use of the Monte Carlo shell model methods [132].

A powerful approach related to systematic variation of specific matrix elements of the shell-model Hamiltonian allows one to look inside the black box of a large-scale diagonalization and understand the roles of individual parts of the many-body Hamiltonian. The deformed shape, as can be concluded from [134], comes from the matrix elements of two-body interaction which describe, with parity conservation, the change of the orbital momentum  $\Delta\ell = \pm 2$  of one of the particles. This is the formal analog of the standard Nilsson scheme [135] with mixing of orbital states of the same parity by the deformed quadrupole mean field; in the shell model the deformation is explicitly generated by the interaction.

In order to study in the shell-model language the influence of the deformation on the level density, we divide the full set of interaction matrix elements into two groups, above mentioned  $\Delta\ell = \pm 2$ , denoted  $V_1$ , and the rest denoted  $V_2$ , with the regulator parameter  $\lambda$ ,

$$H = h + (1 - \lambda)V_1 + \lambda V_2 \quad (82)$$

The evolution of the level density induced by changing the parameter  $\lambda$  is illustrated by Figure 11, [136]. As a typical example we show the mean quadrupole moment of the state  $2_1^+$  and the cumulative number of levels in an odd-odd nucleus  $^{30}\text{P}$  in a function of  $\lambda$ . In fact, due to the deformation effect, the whole Gaussian curve undergoes the shift to the left on the energy axis which is the collective enhancement sought for.

## 7 Constant temperature model

### 7.1 The model

Here we return to a broader discussion of the CTM which has been started in subsection 2.7. Currently this is one of the most popular empirical models well reflecting incoming experimental data. Here the level density is described by a simple exponential expression

$$\rho(E) = \rho_0 e^{E/T}, \quad (83)$$

where the preexponential factor is usually written as

$$\rho_0 = \frac{1}{T} e^{-E_0/T}. \quad (84)$$

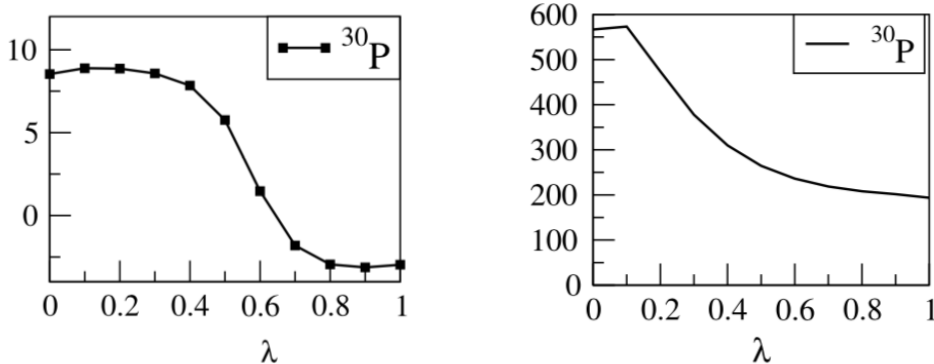


Figure 11: Evolution of the quadrupole moment (left) and the cumulative number of levels (right) under the variation of  $\lambda$  for  $^{30}\text{P}$  (adapted from Ref. [136]).

The analysis of old [62] and new experimental data, including those obtained with the use of the so-called *Oslo method* [159, 160, 161], had shown that this simple description agrees reasonably well with data for many nuclei (up to some excitation energy). We note the faster (exponential) growth of the level density with energy in contrast to the Fermi-gas and semi-empirical models where this growth went slower, as  $\exp(\sqrt{2aE})$ , which requires a value of the empirical parameter  $a$  that grows with energy. The two parameters of this model,  $T$  and  $E_0$ , are to be determined experimentally for each nuclide, and, in principle, for all classes of states with various values of the total spin  $J$  and isospin. Usually only a small fraction of such classes is available in any given experiment.

It is clear that the description (83) cannot be extrapolated to very high excitation energy, especially if one tries to interpret the parameter  $T$  in eq. (83) as a real temperature of the nucleus. The steady exponential growth of the level density leads to the divergence of the statistical partition function (15)

$$Z(\beta) = \int dE \rho(E) e^{-\beta E}. \quad (85)$$

If we assume kind of thermodynamic equilibrium inside a small self-bound system of interacting constituents, the exponential formula stops to be valid close to an excitation energy that corresponds to the thermodynamic temperature  $T_{\text{t-d}} = 1/\beta$  coinciding with  $T$ . It is therefore expected that the

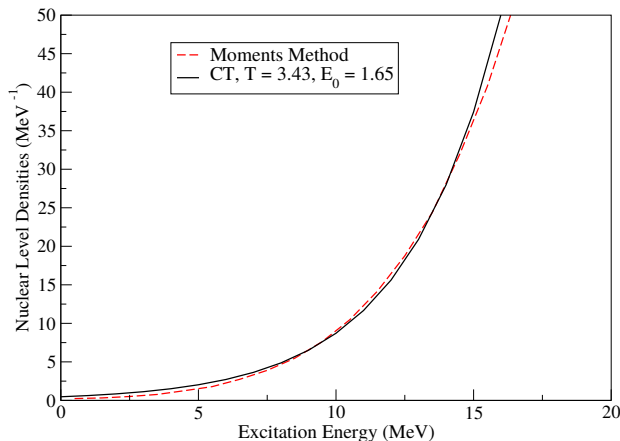


Figure 12: The shell-model level density for  $^{24}\text{Mg}$  (dotted line) and the constant temperature (CT) model (solid line), with parameters  $T = 3.43$  MeV and  $E_0 = 1.65$  MeV for a fitting range 2-15 MeV. Taken from Ref. [167].

CTM description should be matched to that for the heated Fermi-gas at energy that can be estimated in various ways. Such matching was long ago suggested by Gilbert and Cameron [27].

The shell model analysis shows that indeed the CTM description agrees with the exact numerical solution, either found through the full diagonalization, or with the aid of statistical procedures, such as the moments method. Figure 12 taken from [167] shows the total level density for  $^{24}\text{Mg}$  given by the moments method with the full shell-model interaction (it was shown earlier that the result agrees with the shell-model diagonalization and reasonably corresponds to experimental data at least up to  $E \sim 10$  MeV). The fit up to 15 MeV excitation energy is well described by the CTM. A similar situation is shown for  $^{28}\text{Si}$  in Figure 13 [152]. In fact, for practically all nuclei in *sd*- and *pf*-shell model calculations, the CTM agrees well with the numerical results. Such an agreement remains also under variation of the interaction parameters, see examples below. The universality of the approximate description by the CTM allows us to find the behavior of  $T$  as a function of physical characteristics and therefore to clear its physical meaning.

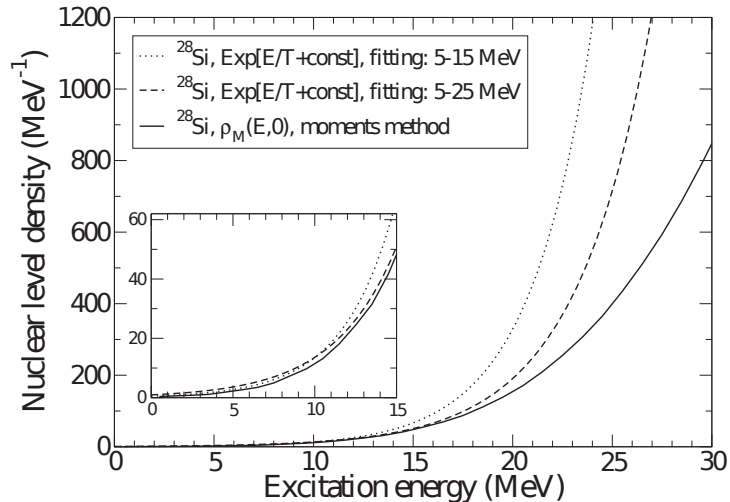


Figure 13: Comparison between global level densities for  $^{28}\text{Si}$  calculated with the moments method (the solid curve) and using the constant temperature for 5 - 15 MeV (the dotted curve) and for 5 - 25 MeV (the dashed curve) energy ranges; the inset presents the magnified low-energy region. Taken from Ref. [152].

## 7.2 Effective temperature

The simple interpretation of the CTM [162, 163, 164] played a significant role in promoting the use of the CTM. The parameter  $T$  was considered as a real temperature of the low-energy part of the nuclear spectrum.  $T$  is kept constant in the energy interval of several MeV (in light nuclei up to 15 MeV) because the nucleus goes through a phase transition from the superfluid phase to the normal Fermi-system. During the transitional phase the latent heat excites the system changing its structure, while the temperature stays fixed. We will call the parameter  $T$  an *effective temperature*. First of all, we show the calculated shell-model value of this parameter for a family of nuclei, see Figure 14.

A noticeable result of this and similar calculations is that, for a given isotopic chain, the effective temperature is minimal in the case of  $N = Z$  for even-even nuclei, or at  $N = Z \pm 1$  for odd- $A$  isotopes, recall the empirical eq. (53) for the Fermi-gas parameter. This seemingly confirms the interpretation based on the pairing phase transition, it is natural to expect that such nuclei are more “frozen”. Nevertheless, we have to mention here that these nuclei

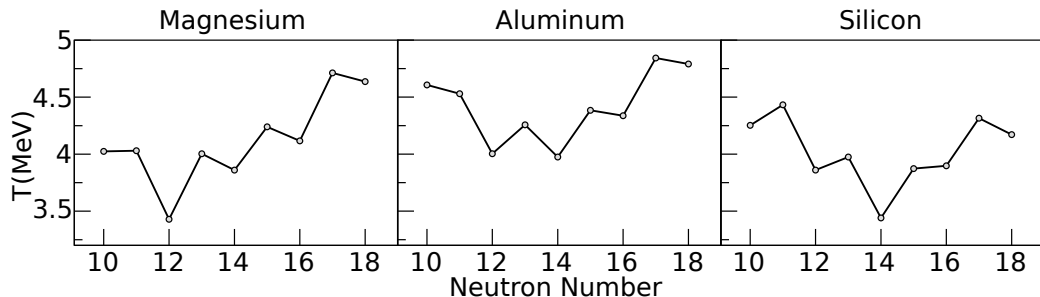


Figure 14: Effective temperature parameter  $T$  for the isotopes of magnesium, aluminum, and silicon. The level density is calculated with the USDB version of the shell model. Adapted from Ref. [167].

are also singled out by other types of correlations, for instance, such as quartic (alpha-type, which could prefer a few-center symmetry of the mean field), and by isospin symmetry (for example, only for  $N = Z$  we have states of isospin zero).

For all  $sd$ -nuclei, the effective temperature values, along with the corresponding parameters  $E_0$  in eq. (84), are calculated and tabulated for various classes of states in Ref. [168]. The found parameters can be used phenomenologically for any treatment of data related to this set of nuclei, with a certain limitation that they are based on a specific version of the shell model which was repeatedly independently checked by the predictions of various physical quantities, especially at relatively low energy, but still accounts for a limited orbital space only.

With exponentially increasing level density (83), we can trace up an analogy with the limiting Hagedorn temperature in particle physics that was discussed in relation with the exponentially proliferating number of particle resonances [162, 169]. If we evaluate the microcanonical entropy  $S$  of the CTM as a function of excitation energy in terms of the cumulative level number,

$$S(E) = \ln \int_0^E dE' \rho(E') = \ln [\rho_0 T (e^{E/T} - 1)], \quad (86)$$

we can introduce the *thermodynamic temperature*

$$T_{\text{t-d}}(E) = \left( \frac{\partial S}{\partial E} \right)^{-1} = T (1 - e^{-E/T}) \quad (87)$$

which starts at zero at the ground state and gradually approaches the effective

temperature  $T$  that plays therefore the role of the *limiting temperature*. As known from old discussions in particle physics, one cannot treat this as the existence of the hottest possible temperature. Rather the system becomes a gas of irregularly interacting constituents – quarks, gluons or strings in particle physics and nucleonic quasiparticles in the heated nucleus. Essentially we gradually come from the ordered regime near the ground state to a heated Fermi-liquid; the parameter  $1/T$  defines the *rate of increase* of the level density as a function of excitation energy. From this viewpoint, the lower value of the effective temperature in  $N = Z$  or close nuclei is a signal of the presence of more active interactions which might prefer different symmetries and reach the chaotic phase faster.

The idea of the phase transition from the superfluid to normal phase [162, 163, 164] seems to be not realistic as we try to show in the next subsection. We can call the process accompanying the growth of excitation energy chaotization, or stochastization, as at some stage the CTM description of the level density should match the general Gaussian shape that is characteristic of quantum chaos, Section 5. The temperature found from the Gaussian description meets the thermodynamic temperature (87) at certain excitation energy slightly different for different nuclei, while the further exponential growth of the level density in the CTM contradicts to thermodynamic stability as follows from (85). This matching was illustrated in [167] by a simple example for  $^{28}\text{Si}$  of a good numerical correspondence between the effective temperature  $T$  and a temperature of the global statistical description at excitation energy 10 MeV where the system reaches the chaotic phase.

### 7.3 Pairing phase transition?

Earlier, Section 6.4, we discussed the role of various components of the interaction in formation of the level density. In particular, the parametrization of eq. (79) allows us to study explicitly the role of the pairing forces. Gradually switching off the pairing force by driving down the parameter  $k_1$  at the fixed value  $k_2 = 1$ , and convincing ourselves that every time the CTM description still stays valid with the changing parameter  $T$ , we come to Figure 15. We see that the effective temperature is essentially constant (in some cases very weakly increases) while pairing practically disappears from the interaction Hamiltonian, both for magnesium and aluminum isotopes. The minimum of  $T$  still corresponds to the same nuclides as in the case of realistic pairing.

Moreover, we can look at the situation in separate classes of states ex-

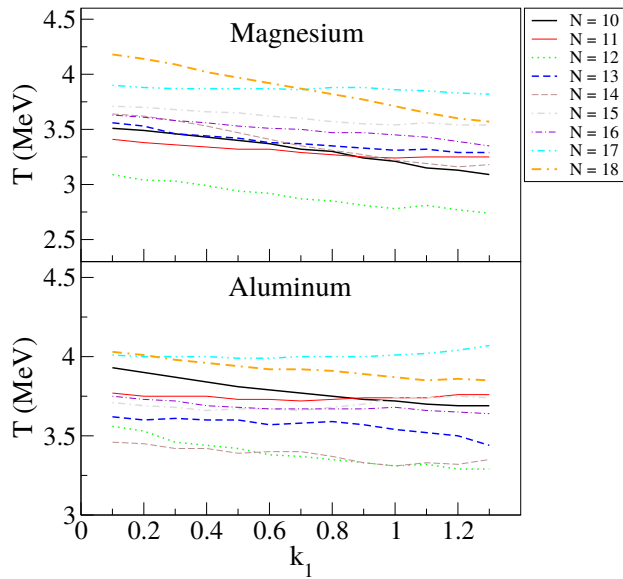


Figure 15: Evolution of the effective temperature parameter  $T$  under variation of the pairing strength  $k_1$  for the isotopes of magnesium and aluminum. Taken from Ref. [167].

pecting the maximum influence of pairing in the cases of low spin. Figure 16 shows the behavior of the effective temperature for states  $J = 0$  and  $J = 2$  in silicon isotopes  $^{28,30}\text{Si}$  as a function of the decreasing parameter  $k_1$ . The effective temperature is again almost constant even for negative values of  $k_1$  (repulsive pairing); the isotope  $^{28}\text{Si}$  has a lower  $T$  for all values of  $k_1$ . Therefore one cannot consider normal attractive pairing as a sole source of the constant effective temperature.

Another variation of the Hamiltonian is given by making all single-particle orbitals degenerate (or simply removing the spin-orbit splitting). The pairing forces then become effectively stronger, pairing gap larger, and therefore one would expect a deeper frozen pair condensate (compare with the superconductivity model in a system with a flat Fermi surface [165, 166]). This would lead to a higher value of the parameter  $T$  necessary to destroy the superfluidity. But the shell-model analysis shows the opposite behavior, the effective temperature goes down, Figure 17. This is what one could expect due to another interpretation: the limiting temperature is lower, and therefore the

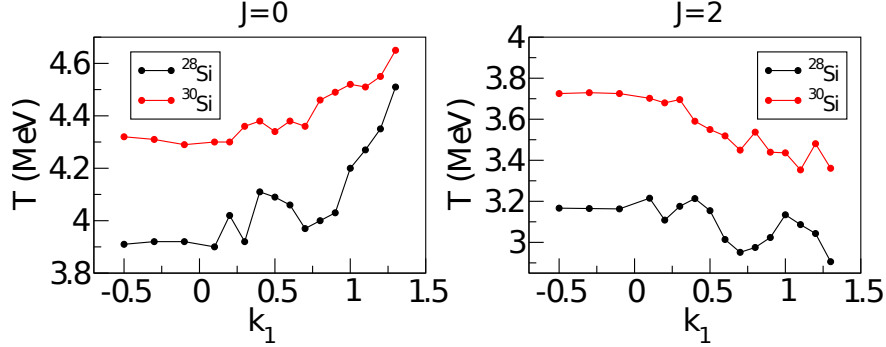


Figure 16: Evolution of the effective temperature parameter  $T$  under variation of  $k_1$  and  $k_2$  for the states  $J = 0$  and  $J = 2$  of  $^{28,30}\text{Si}$ . Adapted from Ref. [167].

rate of chaotization  $1/T$  greater, because of a stronger mixing of many-body degenerate configurations.

In the von Egidy and Bucurescu [174, 175, 176] approach, the  $J$ -dependent nuclear level density is calculated by the approximate formula (see also Eqs. (2)-(4) of Ref. [142] for the correction to the denominator)

$$\rho_{CT}(E, J) = \frac{2J+1}{\sqrt{8\pi}\sigma^3} e^{-J(J+1/2)/(2\sigma^2)} \rho_{CT}(E), \quad (88)$$

with

$$\rho_{CT}(E) = \frac{1}{T} e^{(E-E_0)/T}, \quad (89)$$

where  $\sigma$  is an appropriate spin cutoff parameter that depends on the excitation energy and other isotope specific factors. Here, the assumption is that both parities have the same nuclear level density. This approach has the disadvantage that the constant temperature applies only to the total density of states, and therefore the temperature is not specified for each  $J$  (or parity).

It is possible to introduce a constant temperature formula for each angular momentum  $J$  and each parity  $\pi$ ,

$$\rho_{CT}(E, J, \pi) = \frac{1}{T_{J\pi}} e^{(E-E_{0J\pi})/T_{J\pi}}. \quad (90)$$

A first attempt of using this parametrization was recently reported [177] for some of  $sd$ - and  $fp$ -shell nuclei using the USDA and the GXPF1A Hamiltonians, respectively. Here we add few more data for  $fp$ g nuclei using the JUN45

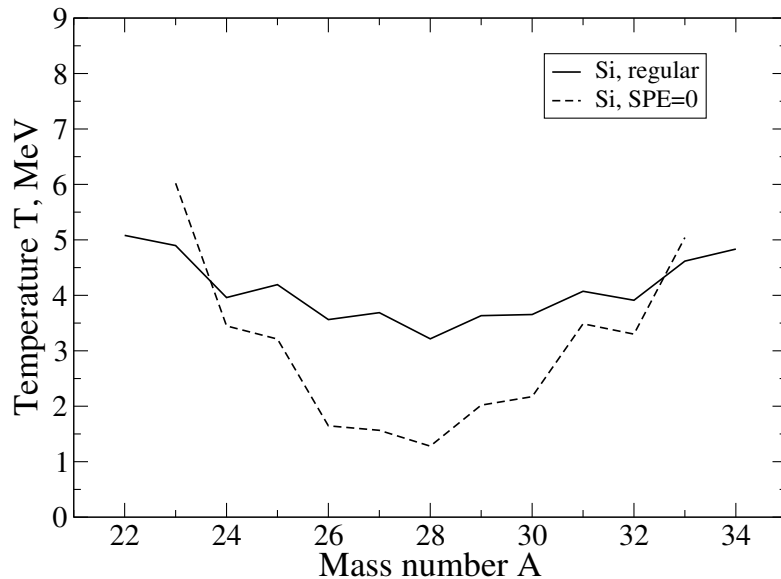


Figure 17: Effective temperature of silicon isotopes with degenerate valence orbitals.

effective Hamiltonian [178]. Figure 18 shows the temperature dependence on the mass number  $A$ , for  $J = 2$  and positive parity. In Ref. [177] it was argued that a constant temperature approach to these individual densities may be better justified than for the density of states that includes subsets from different symmetry representations (e.g. different spins, parities, etc). We found that indeed, the temperatures corresponding to different total angular momenta of the same isotope could be quite different; these temperatures exhibit an odd-even spin effect similar to that found in the low-lying states of nuclei. One could potentially extrapolate the CTM parameters to neighboring isotopes of interest that could be useful for a simple integration of the results of Eq. (90) within reaction codes, such as TALYS.

## 8 Conclusion

The study of the nuclear level density remains an active field of experimental and theoretical research. It goes in parallel to the more detailed studies of known nuclei, steady extension of the nuclear chart approaching the drip lines, and the impressive development of nuclear astrophysics. The knowledge

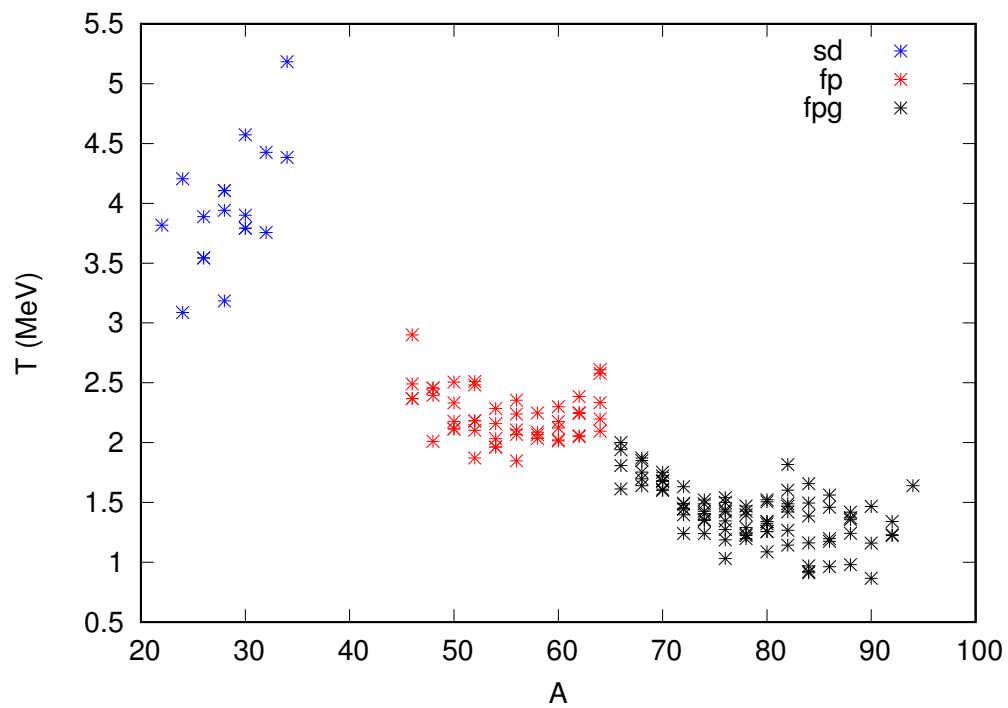


Figure 18: Evolution of  $J=2$ , positive parity temperature vs mass number  $A$  in  $sd$ ,  $fp$ , and  $fpg$  shells.

of the level density is absolutely necessary for treatment of various nuclear processes, including those with excited nuclei as in stellar phenomena.

The empirical information on level density comes mainly from low-energy spectroscopic studies and specific reactions in the vicinity of the neutron threshold. There are traditional approaches trying to combine this information and interpolate between the two energy regions which would make the predictions more reliable. Certainly, such approaches have to be justified from the viewpoint of general nuclear theory. Historically, this theory, in parallel with the progress of computational abilities, was gradually developing. It is however interesting that the first idea concerning the nuclear level density based on the image of the nucleus as a blob of self-bound two-component Fermi-gas survived through more than 80 years of the intellectual maturity of nuclear theory.

The main improvements of the Fermi-gas approach are due to the account for nucleon correlations. The interactions form the self-consistent mean field, spherical or deformed. This determines the single-particle level density at the Fermi surface that would define the nuclear shells and combinatorics of many-particle states at not too high excitation energy. At this point the residual interactions enter the game. The first candidate to this role is the pairing phenomenon. At low energy, the nucleus becomes a drop of superfluid matter; the energy gap distorts the single-particle spectrum close to the Fermi surface, forms the mass differences between even and odd particle numbers, and modifies the collective behavior of the nucleons. Because of the presence of the pair correlations, low-lying collective vibrational modes appear inside the gap, sometimes with observed overtones. In deformed nuclei, collective rotation forms many bands built on intrinsic particle configurations. The rotational moment of inertia, very important for the level density, is determined by the superfluid pairing. Altogether, the low-lying level density becomes enhanced compared to what it would be in the absence of correlations which give rise to the redistribution of stationary states and collective enhancement.

In search for a good theoretical description of the nuclear level density, there were numerous attempts to encounter for the main effects of residual interactions by phenomenological adjustments of the Fermi-gas approach. With typical instruments of adjustment, such as a back-shifted Fermi-gas formula and fitting of the most essential characteristics, including the single-particle level density and spin-cutoff parameter (essentially the effective moment of inertia that determines the level density in the classes of states with

different total nuclear spin), it is frequently possible to reach a decent agreement with selected data. Of course, the absence of physical rules which would predict the values of used parameters and their evolution along the nuclear chart, made the situation not fully satisfactory.

The next theoretical progress was related to the variational methods based on the energy density functionals, for example taken from the Skyrme family. Such models can approximately account for the mean field, pairing, deformation, and other collective phenomena plus single-particle combinatorics. The correctness of description of higher parts of the spectrum is not fully justified. In principle, the energy functionals are typically adjusted by construction for the ground and low-lying states.

One can expect that various versions of the shell model (configuration interaction) can provide the most reliable description of nuclear spectra. The modern fast developing *ab-initio* approaches are still not capable of predicting the nuclear level density for the sufficiently broad energy interval. The Monte Carlo shell model, capable of using considerably larger orbital spaces, was also intensely developed during last twenty years fighting with the sign problem and therefore accounting only for the most regular parts of the interaction.

A widely used practical approach is still based on the standard shell model with effective residual interactions (currently, mainly two-body). The advantage of the shell model is the exact solution of the quantum many-body problem in a finite orbital space. Of course, this feature is at the same time the main restriction for the applicability of the shell model. Above some energy, the states formed on the base of the missed part of the Hilbert space enter the game which makes the predictions of the shell model more and more different from reality. However, the upper energy limit of validity in many cases not only includes the neutron resonance region but also higher energies covering the whole interval important for astrophysical processes and technological applications. The full Hamiltonian of the shell model contains usually more matrix elements than one can reliably find from the low-lying spectroscopy. The level density therefore may provide a quality check for the shell-model Hamiltonian.

Moreover, the experience with the shell model calculations invariably shows the significant role of the matrix elements of the Hamiltonian which are not directly related to the global structure and collective motion. These contributions can be loosely characterized as responsible for the incoherent collision-like interactions which do not influence considerably the mean

field and collective effects. However, these parts of the Hamiltonian contribute considerably to the level density making it smoother and increasing its Gaussian width. They are active participants in creating what is called chaotic dynamics in a many-body system. The nuclear shell model, with the formally exact solution and the richness of physical predictions, is one of the best available testing grounds for many-body quantum chaos. With energy increase, the physical observables come to the qualitative agreement with the limiting predictions of the Gaussian orthogonal ensemble. This can be translated to the thermodynamic language and therefore to entropy and level density. In nuclear shell-model applications, essentially we come to the heated Fermi-liquid with properties expressed through the individual typical wave functions in agreement with the old idea of Landau and Lifshitz now formulated as the eigenfunction thermalization hypothesis. Some predictions of quantum chaos, first of all those of chaotic enhancement of weak effects in the chaotic stage, have been already confirmed experimentally (parity violation, tunneling between different configurations etc.)

The chaotic character of dynamics allows one to reformulate the level density problem in terms of the statistical moments of the many-body Hamiltonian. In practice the first two moments turn out to provide the level density very close to the results of the exact shell-model diagonalization. Of course, being based on the severely truncated orbital space, this method cannot give more than the shell model itself. But it can be more convenient and, with parallelization of computations, cover larger spaces. Another perspective road is related to the recently suggested Lanczos algorithm [170].

An effective instrument of physical studies in the configuration interaction approach is a possibility of numerical experiments by varying the parameters of the Hamiltonian. One can study in this way the change of physical results and evolution of observables hidden in the black box of large-scale diagonalization. Trying to give a working instrument to the practitioners one can use the conventional phenomenological descriptions suggesting the most appropriate values of parameters. Such a study of the Fermi-gas approach provides theoretical values of the standard level density parameter  $a$  and demonstrates the Rosenzweig effect of the shell population. An important detail is in indication of the nuclei where the random coupling of individual spins is violated and therefore the use of the traditional spin cutoff parameter is not valid. Another well known phenomenon, the collective enhancement of low-energy level density due to slow collective modes of rotation and vibrations, is well reproduced by the shell model analysis with artificial deformation of a nu-

cleus through the corresponding change of the interaction parameters. It is important also that the microscopic theory is capable of suggesting the appropriate values of the level density parameters for different classes of states, including those where the existing data are meagre or absent.

Recent experimental and theoretical efforts suggested that the so-called “constant temperature model” with the pure exponential growth of the level density provides a good description of the data. Such a description is often associated with the phase transition where the superfluid pair condensate goes through melting. The theoretical analysis for the *sd*- and *pf*-shells indeed demonstrates that the resulting level density is well described by this model up to some excitation energy. However, varying the pairing strength (even changing the attractive pairing to repulsive) still keeps the same description valid with a small change of the effective temperature parameter. In the text we suggested, with the help of numerous variations of the shell-model parameters, the interpretation of the empirical model in terms of the transition from the regular dynamics near the Fermi-surface to quantum chaos. The effective parameter plays the role of the limiting temperature that defines the rate of the exponential growth of the level density in the process of chaotization of the dynamics. At some energy this growth should match the milder Gaussian behavior of the level density typical for quantum chaos. If this reinterpretation is valid, one can expect the universal applicability of the constant temperature model to self-bound mesoscopic systems with sufficiently strong residual interactions between the constituents.

The whole problem of the microscopic level density is on the crossing of many-body quantum physics, statistical mechanics of small isolated systems, and quantum chaos. With all its practical value, it is also of great theoretical interest which we tried to summarize in this review.

## 9 Acknowledgements

Many results mentioned above were derived in collaboration with R.A. Sen'kov and S. Karampagia. Special gratitude goes to the students who took part at different stages of this work, J. Kaiser, M. Ghita, J. Dissanayake, A. Renzaglia, and A. Berлага. Friendly discussions with B.A. Brown, A.Volya, N. Auerbach, Y. Alhassid, S. Gorieli, S. Grimes, A. Voinov, and the Oslo group were always useful and helpful. For many years the work on level densities was supported by the US NSF grants PHY-9513893, PHY-9901241,

PHY-0070911, PHY-0244453, PHY-0555366, PHY-0758099, PHY-1068217, and PHY-1404442. V.Z. acknowledges the grant from the Binational Science Foundation US-Israel and a useful discussion at the seminar of the Tel Aviv University. M.H. also acknowledges the US DOE grants DE-FC02-09ER41584 and DE-SC0008529.

## References

- [1] N. Bohr, *Nature* **137**, 344 (1936).
- [2] N. Bohr and F. Kalckar, *Kgl. Dansk. Vid. Selsk. Mat.-Fys. Medd.* **14**, No.10 (1937).
- [3] J.M. Blatt and V.F. Weisskopf, *Theoretical Nuclear Physics*, Wiley & Sons, N.Y., 1952; Dover Publications, Mineola, N.Y. 1991.
- [4] I.C. Percival, *J. Phys. B* **6**, L229 (1973).
- [5] C.E. Porter, *Statistical Theories of Spectra: Fluctuations*, Academic Press, N.Y., 1965.
- [6] M.L. Mehta, *Random Matrices*, 3rd ed., Elsevier, Amsterdam, 2004.
- [7] V.K.B. Kota, *Embedded Random Matrix Ensembles in Quantum Physics*, Springer, Cham, 2014.
- [8] H. Bethe, *Phys. Rev.* **50**, 332, 977 (1936).
- [9] H.A. Bethe, *Rev. Mod. Phys.* **9**, 69 (1937).
- [10] A. Bohr and B.R. Mottelson, *Nuclear Structure*, Benjamin, N.Y. 1969.
- [11] J. Bardeen, *Phys. Rev.* **51**, 799 (1937).
- [12] L.D. Landau, *JETP* **7**, 819 (1937) [*Phys. Zs. Sowjetunion* **11**, 556 (1937)].
- [13] L.D. Landau and Ya. Smorodinsky, *Lectures on Nuclear Theory*, Springer, N.Y., 1959.
- [14] J. Frenkel, *Phys. Zs. Sowjetunion* **9**, 533 (1936).
- [15] A.V. Ignatyuk, K.K. Istekov, and G.N. Smirenkin, *Sov. J. Nucl. Phys.* **29**, 450 (1979).
- [16] J. Frenkel, *Sov. Phys. Izvestia*, **1-2**, 233 (1938).
- [17] V. Weisskopf, *Phys. Rev.* **52**, 295 (1937).

- [18] R.H. Fowler, *Statistical Mechanics*, 2nd ed., Cambridge University Press, 1955.
- [19] L.D. Landau and E.M. Lifshitz, *Statistical Physics*, Course of Theoretical Physics, vol. 5, Pergamon Press, Oxford, 1958.
- [20] G.F. Bertsch and L.M. Robledo, *Comp. Phys. Comm.* **185**, 3406 (2014).
- [21] T. Ericson, *Adv. Phys.* **9**, 425 (1960).
- [22] T. Ericson, *Nucl. Phys.* **6**, 62 (1958).
- [23] T. Ericson, *Nucl. Phys.* **8**, 265 (1958).
- [24] T. Ericson, *Nucl. Phys.* **11**, 481 (1959).
- [25] T. Ericson, *Nucl. Phys.* **17**, 250 (1960).
- [26] A. Gilbert, F.S. Chen, and A.G.W. Cameron, *Canad. J. Phys.* **43**, 1248 (1965).
- [27] A. Gilbert and A.G.W. Cameron, *Canad. J. Phys.* **43**, 1446 (1965).
- [28] A.J. Koning, S. Hillaire, and S. Goriely, *Nucl. Phys. A* **810**, 13 (2008).
- [29] V.F. Weisskopf and D.H. Ewing, *Phys. Rev.* **57**, 472 (1940).
- [30] C. Bloch, *Phys. Rev.* **93**, 1094 (1954).
- [31] H. Baba, *Nucl. Phys.* **A159**, 625 (1970).
- [32] T.D. Newton, *Canad. J. Phys.* **34**, 804 (1956).
- [33] N.N. Abdelmalek and V.S. Stavinsky, *Nucl. Phys.* **58**, 601 (1964).
- [34] N. Rosenzweig, *Phys. Rev.* **108**, 817 (1957).
- [35] N. Rosenzweig, in *Nuclear Structure Study with Neutrons*, North-Holland, 1966, p. 309.
- [36] S. Bjornholm, A. Bohr, and B. R. Mottelson, in *Physics and Chemistry of Fission*, 1973, Vol. I, IAEA, Vienna (1974), p. 303, 367.
- [37] M. Horoi, B.A. Brown and V. Zelevinsky, *Phys. Rev. Lett.* **87** (2001) 062501.
- [38] S.T. Belyaev and V.G. Zelevinsky, *Yad. Phys.* **11**, 741 (1970) [*Sov. J. Nucl. Phys.* **11**, 416 (1970)].
- [39] S.T. Belyaev and V.G. Zelevinsky. *Yad. Fiz.* **17**, 525 (1973) [*Sov. J. Nucl. Phys.* **17**, 269 (1973)].

- [40] J.M.B. Lang and K.J. Le Couter, Proc. Phys. Soc. **A67**, 586 (1954).
- [41] A. V. Malyshev, Sov. Phys. JETP **18**, 221 (1969).
- [42] A.V. Malyshev, *Nuclear Structure and Level Density*, Atomizdat, Moscow, 1969 /in Russian/.
- [43] C.T. Hibdon, Phys. Rev. **114**, 179 (1959).
- [44] C.T. Hibdon, Phys. Rev. **124**, 500 (1961).
- [45] J. R. Huizenga and R. Vandenbosch, Phys. Rev. **120**, 1305 (1960).
- [46] R. Vandenbosch and J. R. Huizenga, Phys. Rev. **120**, 1313 (1960).
- [47] H.K. Vonach, R. Vandenbosch, and J.R. Huizenga, Nucl. Phys. **60**, 70 (1964).
- [48] T. Ericson and V. Strutinsky, Nucl. Phys. **8**, 284 (1958).
- [49] A.C. Douglas and N. MacDonald, Nucl. Phys. **13**, 382 (1959).
- [50] D.W. Lang, Nucl. Phys. **26**, 434 (1961).
- [51] C.E. Porter and R.G. Thomas, Phys. Rev. **104**, 483 (1956).
- [52] I.I. Gurevich and M.I. Pevzner, JETP **31**, 162 (1956); Physica **22**, 1132 (1956).
- [53] H.W. Broek, Phys. Rev. **124**, 233 (1961).
- [54] H. Nakada and Y. Alhassid, Phys. Rev. Lett. **79**, 2939 (1997).
- [55] M.G. Mayer, Phys. Rev. **74**, 235 (1948).
- [56] M.G. Mayer and J.H.D. Jensen, *Elementary Theory of Nuclear Structure*, N.Y. 1955.
- [57] J. Bardeen, L.N. Cooper, and J.R. Schriffer, Phys. Rev. **106**, 162 (1957); **108**, 1175 (1957).
- [58] A. Bohr, B.R. Mottelson, and D. Pines, Phys. Rev. **110**, 936 (1958).
- [59] S.T. Belyaev, Kgl. Dansk. Vid. Selsk. Mat.-Fys. Medd. **31**, No. 11 (1959).
- [60] P.E. Nemirovsky and Yu.V. Adamchuk, Nucl. Phys. **39**, 553 (1962).
- [61] A. Stolovy and J.A. Harvey, Phys. Rev. **108**, 353 (1957).
- [62] P.J. Brancazio and A.G.W. Cameron, Can. J. Phys. **47**, 1029 (1969).
- [63] P. Demetriou and S. Goriely, Nucl. Phys. A **695**, 95 (2001).

- [64] W. Dilg, W. Schantl, H. Vonach, and M. Uhl, Nucl. Phys. A **217**, 269 (1973).
- [65] J.R. Huizenga and L.G. Moretto, Annu. Rev. Nucl. Sci. **22**, 427 (1972).
- [66] S.I. Al-Quraishi, S.M. Grimes, T.N. Massey, and D.A. Resler, Phys. Rev. C **63**, 065803 (2001).
- [67] M. Horoi and V. Zelevinsky, Phys. Rev. C **75**, 054303 (2007).
- [68] V. Zelevinsky and A. Volya, *Physics of Atomic Nuclei*, Wiley VCH, Weinheim, 2017.
- [69] R.M. Rockmore, Phys. Rev. **116**, 469 (1959).
- [70] T. Belgya *et al.*, IAEA-TECDOC-1506, Handbook for calculations of nuclear reactions data: Reference Input Parameter Library-2, IAEA, Vienna, 2005; <http://www-nds.iaea.org/RIPL-2/>.
- [71] S. Hillaire, J.P. Delaroche, and A.J. Koning, Nucl. Phys. A **632**, 417 (1998).
- [72] S. Hillaire, J.P. Delaroche, and M. Girod, Eur. Phys. J. A **12**, 169 (2001).
- [73] S.T. Belyaev, *Collective Excitations in Nuclei*, Gordon and Breach, N.Y., 1968.
- [74] A.L. Goodman, Adv. Nucl. Phys. **11**, 263 (1979).
- [75] J. Libert, M. Girod, and J.P. Delaroche, Phys. Rev. C **60**, 054301 (1999).
- [76] J. Decharge and D. Gogny, Phys. Rev. C **21**, 1568 (1980).
- [77] J.-F. Berger, M. Girod, and G. Gogny, Comp. Phys. Comm. **63**, 365 (1991).
- [78] S.T. Belyaev, Nucl. Phys. **24**, 322 (1961).
- [79] S. Goriely, S. Hillaire, and A.J. Koning, Phys. Rev. C **78**, 064307 (2008).
- [80] S. Hillaire and S. Goriely, Nucl. Phys. A **779**, 63 (2006).
- [81] S. Hillaire, M. Girod, S. Goriely, and A.J. Koning, Phys. Rev. C **86**, 064317 (2012).
- [82] S. Goriely, S. Hillaire, M. Girod, and S. Pery, Phys. Rev. Lett. **102**, 242501 (2009).
- [83] G. Sugiyama and S.E. Koonin, Ann. Phys. (N.Y.) **168**, 1 (1986).
- [84] S.E. Koonin, D.J. Dean, and K. Langanke, Phys. Rep. **278**, 2 (1997).

- [85] T. Otsuka, M. Honma, T. Mizusaki, N. Shimizu, and Y. Utsuno, *Prog. Part. Nucl. Phys.* **47**, 319 (2001).
- [86] G.H. Lang, C.W. Johnson, S.E. Koonin, and W.E. Ormand, *Phys. Rev. C* **48**, 1518 (1993).
- [87] C.W. Johnson, S.E. Koonin, G.H. Lang, and W.E. Ormand, *Phys. Rev. Lett.* **69**, 3157 (1992).
- [88] W.E. Ormand, *Phys. Rev. C* **56**, R1678 (1997).
- [89] J. Hubbard, *Phys. Lett.* **3**, 77 (1959).
- [90] R.D. Stratonovich, *Dokl. Akad. Nauk* **115**, 1907 (1957) [*Sov. Phys. Dokl.* **2**, 416 (1958)].
- [91] N. Metropolis, A.W. Rosenbluth, M.N. Rosenbluth, A.M. Teller, and E. Teller, *J. Chem. Phys.* **21**, 1087 (1953).
- [92] W.E. Ormand, D.J. Dean, C.W. Johnson, G.H. Lang, and S.E. Koonin, *Phys. Rev. C* **49**, 1422 (1994).
- [93] Y. Alhassid, D.J. Dean, G. Lang, S.E. Koonin and W.E. Ormand, *Phys. Rev. Lett.* **72**, 613 (1994).
- [94] W.A. Richter, M.G. Wan der Merwe, R.E. Julies, and B.A. Brown, *Nucl. Phys.* **A523**, 325 (1991).
- [95] H. Nakada and Y. Alhassid, *Phys. Lett. B* **436**, 231 (1998).
- [96] C.C. Lu, L.C. Vaz, and J.R. Huizenga, *Nucl. Phys.* **A190**, 229 (1972).
- [97] Y. Alhassid, S. Liu, and H. Nakada, *Phys. Rev. Lett.* **83**, 4265 (1999).
- [98] Y. Alhassid, G.F. Bertsch, and L. Fang, *Phys. Rev. C* **68**, 044302 (2003).
- [99] S. Shlomo, V.M. Kolomietz, and H. Dejbakhsh, *Phys. Rev. C* **55**, 1972 (1997).
- [100] Y. Alhassid, G.F. Bertsch, L. Fang, and S. Liu, *Phys. Rev. C* **72**, 064326 (2005).
- [101] Y. Alhassid, S. Liu, and H. Nakada, *Phys. Rev. Lett.* **99**, 162504 (2007).
- [102] Y. Alhassid, L. Fang, and H. Nakada, *Phys. Rev. Lett.* **101**, 082501 (2008).
- [103] Y. Alhassid in “Emergent Phenomena in Atomic Nuclei from Large-Scale Modeling : a Symmetry-guided Perspective”, ed. K.D. Launey, World Scientific, 2018.

- [104] Y. Alhassid, M. Bonett-Matiz, S. Liu, and H. Nakada, Phys. Rev. C **92**, 024307 (2015).
- [105] Y. Alhassid, L. Fang, and H. Nakada, J. Phys. Conf. Ser., **267**, 012033 (2011).
- [106] L. F. Santos, M. I. Dykman, M. Shapiro, and F. M. Izrailev, Phys. Rev. A **71**, 012317 (2005).
- [107] T.A. Brody, J. Flores, J.B. French, P.A. Mello, A. Pandey, and S.S.M. Wong, Rev. Mod. Phys. **53**, 385 (1981).
- [108] G.F. Bertsch and R.A. Broglia, *Oscillations in Finite Quantum Systems*, Cambridge University Press, Cambridge, 1994.
- [109] J. Armstrong, S. Aaberg, S.M. Reimann, and V. Zelevinsky, Phys. Rev. E **86**, 066204 (2012).
- [110] V. Zelevinsky, B.A. Brown, N. Frazier, and M. Horoi, Phys. Rep. **276**, 85 (1996).
- [111] H. A. Weidenmüller and G. E. Mitchell, Rev. Mod. Phys. **81**, 539 (2009).
- [112] V. Zelevinsky and A. Volya, Phys. Scripta **91**, 033996 (2016).
- [113] O.P. Sushkov and V.V. Flambaum, Usp. Fiz. Nauk **136**, 3 (1982) [Sov. Phys. Usp. **25**, 1 (1982)].
- [114] V.P. Alfimenkov, S.B. Borzakov, Vo Van Thuan, Yu.D. Mareev, L.B. Pikelner, A.S. Khrykin, and E.I. Sharapov, Nucl. Phys. A **398**, 93 (1983).
- [115] C.M. Frankle *et al.*, Phys. Rev. Lett. **67**, 564 (1991).
- [116] B.E. Crawford *et al.* (*TRIPLE collaboration*), Phys. Rev. C **58**, 1225 (1990).
- [117] L.Y. Lowie *et al.*, Phys. Rev. C **59**, 1119 (1999).
- [118] G.V. Danilyan, Sov. Phys. Usp. **23**, 323 (1980).
- [119] G.A.Petrov, G.V. Valskii, A.K. Petukhov, A.Ya. Alexandrovich, Yu.S. Pleva, V.E. Sokolov, A.B. Laptev, and O.A. Scherbakov, Nucl. Phys. A **502**, 297 (1989).
- [120] A. Müller, Phys. Rev. C **45**, 1955 (1992).
- [121] A. Koetzle, P. Jesinger, F. Goennenwein, G.A. Petrov, A.M. Gagarsky, G. Danilyan, O. Zimmer, and V.V. Nesvishevsky, Nucl. Inst. Methods A **440**, 750 (2000).

- [122] V. Zelevinsky, *Annu. Rev. Nucl. Part. Sci.* **46**, 237 (1996).
- [123] F. Borgonovi, F.M. Izrailev, L.F. Santos, and V.G. Zelevinsky, *Phys. Rep.* **626**, 1 (2016).
- [124] T. Mori, T.N. Ikeda, E. Kaminishi, and M. Ueda, arXiv: 1712.08790.
- [125] J.M. Deutsch, *Phys. Rev. A* **43**, 2046 (1991).
- [126] M. Srednicki, *Phys. Rev. E* **50**, 888 (1994).
- [127] T. Yoshizawa, E. Iyoda, and T. Sagawa, arXiv:1712.07289,
- [128] N.S. Krylov, *Works on the foundations of statistical physics*, Princeton University Press, 1979.
- [129] L. Van Hove, *Physica* **21**, 901 (1955); **22**, 343 (1956).
- [130] V.V. Flambaum, A.A. Gribakina, G.F. Gribakin, and M.G. Kozlov, *Phys. Rev. A* **50**, 267 (1994).
- [131] V.V. Flambaum and F.M. Izrailev, *Phys. Rev. E* **56**, 5144 (1997).
- [132] C.Özen, Y. Alhassid, and H. Nakada, *Phys. Rev. Lett.* **110**, 042502 (2013).
- [133] C.Özen, Y. Alhassid, and H. Nakada, *Phys. Rev. C* **91**, 034329 (2015).
- [134] M. Horoi and V. Zelevinsky, *Phys. Rev. C* **81**, 034306 (2010).
- [135] S.G. Nilsson, *Kgl. Dansk. Vid. Selsk. Mat.-Fys. Medd.* **29**, No. 16 (1955).
- [136] S.Karampagia, A.Renzaglia, and V.Zelevinsky, *Nucl. Phys.* **A962**, 46 (2017).
- [137] J.B. French and V.K.B. Kota, *Phys. Rev. Lett.* **51**, 2183 (1983).
- [138] S.S.M. Wong, *Nuclear Statistical Spectroscopy*, Oxford University Press, 1986.
- [139] V.K.B. Kota and R.U. Haq, eds., *Spectral Distributions in Nuclei and Statistical Spectroscopy* (World Scientific, Singapore, 2010).
- [140] N. Auerbach and V. Zelevinsky, *Rep. Prog. Phys.* **74**, 106301 (2011).
- [141] A. Volya, H.A. Weidenmüller, and V. Zelevinsky, *Phys. Rev. Lett.* **115**, 052501 (2015).
- [142] M. Horoi, J. Kaiser, and V. Zelevinsky, *Phys. Rev. C* **67**, 054309 (2003).

- [143] N. Frazier, B.A. Brown and V. Zelevinsky. Phys. Rev. C **54** (1996) 1665.  
Reprinted in: V.K.B. Kota and R.U. Haq, eds., *Spectral Distributions in Nuclei and Statistical Spectroscopy* (World Scientific, Singapore, 2010) p. 557.
- [144] M. Horoi, M. Ghita, and V. Zelevinsky, Phys. Rev. C **69**, 041307(R) (2004).
- [145] R.A. Sen'kov and M. Horoi, Phys. Rev. C **82**, 024304 (2010).
- [146] R.A. Sen'kov, M. Horoi, and V. Zelevinsky, Comp. Phys. Comm. **184**, 215 (2013).
- [147] M. Horoi, A. Volya, and V. Zelevinsky, Phys. Rev. Lett. **82**, 2064 (1999).
- [148] M. Horoi, B.A. Brown, and V. Zelevinsky, Phys. Rev. C **65**, 027303 (2002).
- [149] C. Jacquemin, Z. Phys. A **303**, 135 (1981).
- [150] P. Van Isacker, Phys. Rev. Lett. **89**, 262502 (2002).
- [151] M. Horoi and V. Zelevinsky, Phys. Rev. Lett. **98**, 262503 (2007).
- [152] R. Sen'kov and V. Zelevinsky, Phys. Rev. C **93**, 064304 (2016).
- [153] B.A. Brown and B.H. Wildenthal, Annu. Rev. Nucl. Part. Sci. **38**, 29 (1988).
- [154] <http://www-astro.ulh.ac.he/bruslib>
- [155] A. Volya, V. Zelevinsky, and B.A. Brown, Phys. Rev. C **65**, 054312 (2002).
- [156] V. Zelevinsky, D. Mulhall, and A. Volya, Phys. At. Nucl. **64**, 525 (2001).
- [157] G. Rohr, Z. Phys. A **318**, 299 (1984).
- [158] P.J. Brancazio and A.G.W. Cameron, Can. J. Phys. **47**, 1029 (1969).
- [159] A.V. Voinov, B.M. Oginni, S.M. Grimes, C.R. Brune, M. Guttormsen, A.C. Larsen, T.N. Massey, A. Schiller, and S. Siem, Phys. Rev. C **79**, 031301 (2009).
- [160] M. Guttormsen *et al.*, Phys. Rev. C **88**, 024307 (2013).
- [161] M. Guttormsen *et al.*, Phys. Rev. C **89**, 014302 (2014).

- [162] L.G. Moretto, Nucl. Phys. A **243**, 77 (1975).
- [163] L. G. Moretto, A. C. Larsen, F. Giacoppo, M. Guttormsen, and S. Siem, J. Phys.: Conf. Series, **580**, 012048 (2015).
- [164] L.G. Moretto, A.C. Larsen, M. Guttormsen, and S. Siem, AIP Conf. Proc. **1681**, 040011 (2015).
- [165] V. A. Khodel and V. R. Shaginyan, JETP Lett. **51**, 553 (1990).
- [166] V.A. Khodel, V.R. Shaginyan, V.V. Khodel, Phys. Rep. **249**, 1 (1994).
- [167] V. Zelevinsky, S. Karampagia, and A. Berlaga, Phys. Lett. B **783**, 428(2018).
- [168] S. Karampagia, R.A. Sen'kov, and V. Zelevinsky, Atomic Data and Nuclear Data Tables **120**, Pages 1-120 (2018).
- [169] J.J. Atick and E. Witten, Nucl. Phys. B **310**, 291 (1988).
- [170] B.A. Brown, private communication.
- [171] M. Horoi and R. Senkov, in NUCLEI IN COSMOS XI (2010), vol. NIC XI of Proceedings of Science, p. 222, <https://pos.sissa.it/100/222/> .
- [172] <http://www.talys.eu> .
- [173] A. V. Voinov, S. M. Grimes, C. R. Brune, M. J. Hornish, T. N. Massey, and A. Salas, Phys. Rev. C **76**, 044602 (2007).
- [174] T. von Egidy and D. Bucurescu, Phys. Rev. C **72**, 044311 (2005).
- [175] T. von Egidy and D. Bucurescu, Phys. Rev. C **80**, 054310 (2009).
- [176] T. von Egidy and D. Bucurescu, in *Advanced many-body and statistical methods in mesoscopic systems* (2012), vol. 338 of *Journal of Physics Conference Series*, p. 012028.
- [177] M. Horoi and J. Dissanayake, AIP Conf. Proc. **1912**, 020006 (2017), [arXiv:1710.00752](https://arxiv.org/abs/1710.00752).
- [178] M. Honma and T. Otsuka and T. Mizusaki and M. Hjorth-Jensen, Phys. Rev. C, **80**, 064323 (2009).